Office of Naval Research

Contract N50RI-76 • Task Order No.1 • NR-071-012

SOME SPIN WAVE PROPERTIES OF FERRIMAGNETIC AND ANTIFERROMAGNETIC SIMPLE CUBIC CRYSTALS

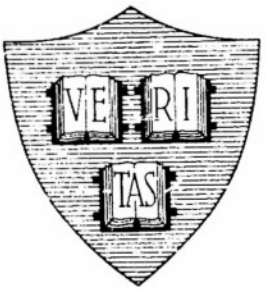

By

J. S. Kouvel and Harvey Brooks

May 20, 1954

Technical Report No. 198

Cruft Laboratory
Harvard University
Cambridge, Massachusetts

Office of Naval Research

Contract N5ori-76

Task Order No. 1

NR-071-011

Technical Report

on

Some Spin Wave Properties of Ferrimagnetic and Antiferromagnetic Simple Cubic Crystals

by

J. S. Kouvel and Harvey Brooks

May 20, 1954

The research reported in this document was made possible through support extended Cruft Laboratory, Harvard University, jointly by the Navy Department (Office of Naval Research), the Signal Corps of the U. S. Army, and the U. S. Air Force, under ONR Contract N5ori-76, T. O. 1.

Technical Report No. 198

Cruft Laboratory

Harvard University

Cambridge, Massachusetts

TR198

Some Spin Wave Properties of Ferrimagnetic and Antiferromagnetic Simple Cubic Crystals

by

J. S. Kouvel and Harvey Brooks

Cruft Laboratory, Harvard University

Cambridge, Massachusetts

1. Introductory Remarks

Several theories on the electronic spin resonance[1] in ferrimagnetic and antiferromagnetic media have been recently developed to a point where their results may be readily compared with experiment. These have all been based on simple semiclassical principles, and hence, must await confirmation from more rigorous, quantum mechanical work, also now in progress.[2] The main purpose of this paper is a semiclassical spin wave treatment of certain "bulk" properties (namely, the specific heat and saturation magnetization at low temperatures) of a simple cubic ferrimagnetic or antiferromagnetic crystal; the results, we hope, will also be amenable to at least qualitative comparison with experiment. For the sake of simplicity, this study is confined to a simple cubic single crystal which we postulate to have a single axis of magnetic anisotropy (along a cube edge) instead of the cubic anisotropy generally associated with such a crystal. The effects of a uniform magnetic field applied along the anisotropy axis are studied for both ferrimagnetic and antiferromagnetic cases; moreover, for the latter case, the situation in which the field is applied perpendicular to the anisotropy axis is also considered.

Since our results can be readily made to apply to the ferromagnetic case of the simple cubic model, we are able to check them directly with the results of previous spin wave analyses of the ferromagnetic problem. Consequently, it becomes possible to trace the similarities and differences of the "bulk" spin wave properties of all three cases: ferromagnetic, ferrimagnetic, and antiferromagnetic.

2. The Ferrimagnetic Case

The atomic arrangement in our simple cubic model is ordered with respect to the net electronic spin per atom in the manner shown in Figure 1. The ground state of this system is assumed to be such that the electronic spin of each atom of sublattice (1) is directed upwards (in the z direction) while the spin of each atom of sublattice (2) is directed downwards. Though there is no rigorous theoretical justification for this assumption, it is hoped that the arguments of Anderson and others[2] for very nearly this type of long-range order in the ground state of a simple cubic antiferromagnetic may be also applicable in the ferrimagnetic case. In fact, these arguments, being basically classical, should have increased validity for large atomic spins, which is usually the case for ferrimagnetics. Furthermore, Néel's phenomenological theory[3] of the saturation magnetization of ferrites, which has enjoyed remarkable agreement with experiment, is firmly based on an antiparallel alignment of unequal atomic spins.

The energy of negative exchange interaction which is responsible for this antiparallel alignment may be expressed as

$$2J \sum_{i,j} \underline{S}_i \cdot \underline{S}_j$$

so that J, the negative of the exchange integral, is a positive quantity. For the present, we shall consider only nearest neighbor exchange interactions; the additional effects of next-to-nearest neighbor interactions are discussed in Appendix A.

An axial magnetic anisotropy which tends to direct the spins along the z-axis, is assumed to have an energy associated with it as follows:

$$\sum_j K_j S_j \sin^2 \theta_j \quad \text{or} \quad \sum_j \frac{K_j}{S_j} \underline{S}_j \cdot (\underline{S}_{xj} + \underline{S}_{yj})$$

where K_j is the anisotropy energy per unit spin of S_j, and θ_j is the angle $\underline{S}_j$ makes with the z-axis.

Furthermore, the system is subjected to a uniform magnetic field, H, in the z direction, which gives rise to the energy,

$$-\underline{H} \cdot \sum_j g_j \beta \underline{S}_j$$

where β is the Bohr magneton and g_j is the spectroscopic splitting factor for the electronic magnetic moment of the jth atom.

The sum of these three energy terms is taken to be the total Hamiltonian of the system. Throughout this report, we have thus neglected the effects of magnetic dipole-dipole interactions between spins, except insofar as they are included phenomenologically in the anisotropy energy;[4] for a structure having the simple cubic symmetry shown in Figure 1, they may be expected to be small.

The equation of motion of the ℓth spin vector may be written as

$$\hbar \dot{\underline{S}}_\ell = -2J\underline{S}_\ell \times \sum_j \underline{S}_j - \frac{2K_\ell}{S_\ell} \underline{S}_\ell \times (\underline{S}_{x\ell} + \underline{S}_{y\ell}) + g_\ell \beta \underline{S}_\ell \times \underline{H} \quad . \tag{2.1}$$

Indicating the two sublattices by superscripts (1) and (2), we express the spin vectors in their rectangular components as follows:

$$\underline{S}^{(1)} = \hat{j}_x S_x^{(1)} + \hat{j}_y S_y^{(1)} + \hat{j}_z S_1 \tag{2.2a}$$

$$\underline{S}^{(2)} = \hat{j}_x S_x^{(2)} + \hat{j}_y S_y^{(2)} - \hat{j}_z S_2 \quad . \tag{2.2b}$$

The z components of spin, to a first approximation, are considered to be invariant in time and space. This is equivalent to neglecting terms quadratic in the S_x's and S_y's. Furthermore, we assume that all x and y spin components are expressible in the form

$$S_x^{(n)}(x,y,z,t) = S_x^{(n)}(a_x, a_y, a_z, t) \exp\left\{2\pi i (a_x x + a_y y + a_z z)/a\right\} \tag{2.3}$$

where a is the distance between nearest neighbor atoms and $\underline{a}_x + \underline{a}_y + \underline{a}_z = \underline{a}$ is a dimensionless phase vector (corresponding to Anderson's[2] $\underline{\lambda}/2\pi$ and to Herring and Kittel's[5] $\underline{k}a/2\pi$). The equations of motion for the x and y spin components are then found to be

$$\hbar\dot{S}_x^{(1)} = 12JS_1\gamma_a S_y^{(2)} + (12JS_2 + 2K_1 + g_1\beta H)S_y^{(1)} \qquad (2.4a)$$

$$\hbar\dot{S}_x^{(2)} = -12JS_2\gamma_a S_y^{(1)} + (-12JS_1 - 2K_2 + g_2\beta H)S_y^{(2)} \qquad (2.4b)$$

$$\hbar\dot{S}_y^{(1)} = -12JS_1\gamma_a S_x^{(2)} + (-12JS_2 - 2K_1 - g_1\beta H)S_x^{(1)} \qquad (2.4c)$$

$$\hbar\dot{S}_y^{(2)} = 12JS_2\gamma_a S_x^{(1)} + (12JS_1 + 2K_2 - g_2\beta H)S_x^{(2)} \qquad (2.4d)$$

where

$$\gamma_a = (\cos 2\pi a_x + \cos 2\pi a_y + \cos 2\pi a_z)/3 \quad .$$

We now assume that the time dependence of the x and y spin components is of the form

$$S_x^{(n)} + iS_y^{(n)} = S_+^{(n)} e^{-i\omega t} \qquad (2.5a)$$

$$S_x^{(n)} - iS_y^{(n)} = S_-^{(n)} e^{i\omega t} \quad . \qquad (2.5b)$$

By means of (2.5a), (2.4a) is combined with (2.4c), and (2.4b) with (2.4d) to yield

$$\hbar\omega S_+^{(1)} = 12JS_1\gamma_a S_+^{(2)} + (12JS_2 + 2K_1 + g_1\beta H)S_+^{(1)} \qquad (2.6a)$$

$$\hbar\omega S_+^{(2)} = -12JS_2\gamma_a S_+^{(1)} + (-12JS_1 - 2K_2 + g_2\beta H)S_+^{(2)} \qquad (2.6b)$$

[(2.5b) leads to the same equations with the subscripts + replaced by -] from which the following solutions for the frequencies are immediately obtained:

$$\begin{aligned}\hbar\omega = {} & -6J(S_1 - S_2) + K_1 - K_2 + (g_1 + g_2)\beta H/2 \\ & \pm \Big[\{6J(S_1 - S_2)\}^2 \\ & + \{K_1 + K_2 + (g_1 - g_2)\beta H/2\} \{12J(S_1 + S_2) + K_1 + K_2 + (g_1 - g_2)\beta H/2\} \\ & + (12J)^2 S_1 S_2 (1 - \gamma_a^2) \Big]^{1/2} \end{aligned} \qquad (2.7)$$

At very low temperatures, where the spin wave theory is most likely to be valid, only the spin waves of very long wavelength compared to the

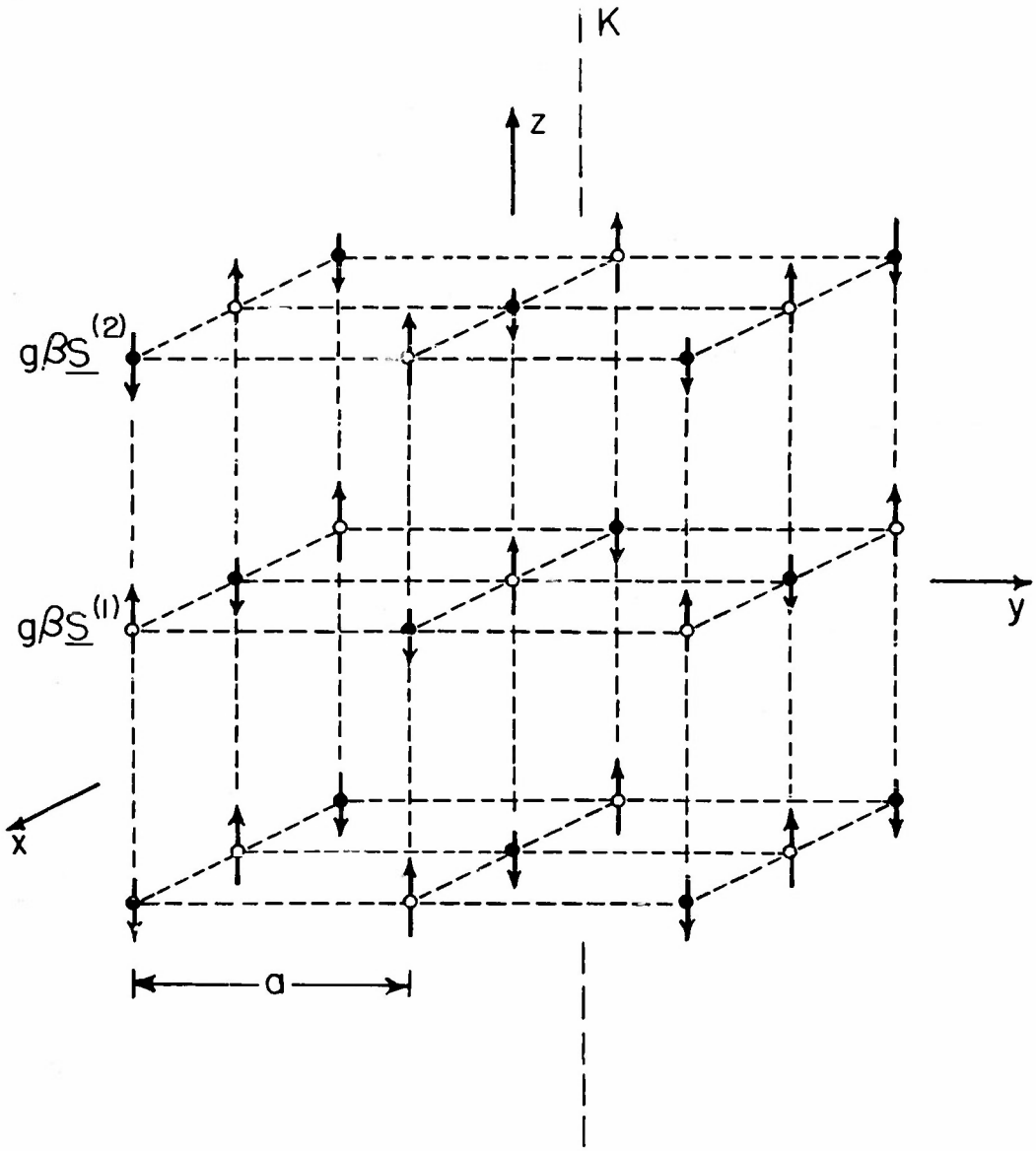

FIGURE 1

lattice spacing may be expected to be excited appreciably. Hence, a will range over very small values and

$$\gamma_a \simeq 1 - \frac{2\pi^2}{3} a^2 \quad \text{or} \quad 1 - \gamma_a^2 \simeq \frac{4\pi^2}{3} a^2 \quad . \tag{2.8}$$

Moreover, for a ferrimagnetic with a reasonably high Curie temperature, $6J(S_1-S_2)$ is substantially larger than the terms in (2.7) that contain the anisotropy constants, the applied field, or a. It follows that the frequencies of the two modes are very different from each other. We can ignore the higher or "optical" mode since its contributions to the specific heat and to the temperature change of magnetization are negligible at temperatures well below the Curie point, and consider only the lower or "acoustical" mode (corresponding to the choice of the positive sign in (2.7)). It should be noted that a discrepancy between the g-factors of the two sublattices causes an apparent field-dependent increase of the anisotropy; this was recently discussed by Wangsness[6] in his analysis of ferrimagnetic resonance. Conversely, a difference between the two anisotropy constants shows up as an apparent increase of the g-factors (or of the external field). Hence, keeping the possibility of these effects in mind, we proceed to simplify (2.7) by setting $K_1 = K_2 = K$ and $g_1 = g_2 = g$. We then expand the square root in (2.7) and obtain for the "acoustical" mode

$$\hbar\omega \simeq g\beta H + 2K\left\{\frac{S_1+S_2+K/6J}{S_1-S_2}\right\} + \frac{12JS_1S_2}{S_1-S_2}\left(\frac{4\pi^2}{3} a^2\right) \quad . \tag{2.9}$$

For comparison, the spin vibrational frequencies for a ferromagnetic simple cubic structure may be readily obtained from (2.7) by setting $S_1 = -S_2 = S$, $K_1 = -K_2 = K$, $g_1 = g_2 = g$, and $-J = J'$, in which case it is found that

$$\hbar\omega \simeq g\beta H + 2K + 6J'S\left(\frac{4\pi^2}{3} a^2\right) \quad . \tag{2.10}$$

Thus, except for the generally small effects of anisotropy and applied magnetic fields, ω is proportional to a^2 in both the ferrimagnetic and ferromagnetic cases. Such a relationship between ω and a, as has been shown in previous discussions of the ferromagnetic case, leads directly

to a $T^{3/2}$ law of the specific heat and of the decrease of saturation magnetization. We shall now make use of equation (2.9) to derive the actual expressions for these properties of a ferrimagnetic.

Quantizing the normal modes of our classical spin wave problem, we are led to the following expression for the specific heat per atom:[7]

$$C_a = k\int_{a=0}^{\infty} \frac{\xi^2 e^{\xi}\,(4\pi a^2 da)}{(e^{\xi}-1)^2} \tag{2.11}$$

where $\xi = \hbar\omega/kT$. By means of (2.9), (2.11) is transformed to

$$C_a = \frac{k}{4\pi^2}\left\{\frac{(S_1-S_2)kT}{4JS_1S_2}\right\}^{3/2} \int_{\xi_{H'}}^{\infty} \frac{e^{\xi}\,\xi^2(\xi-\xi_{H'})^{1/2}}{(e^{\xi}-1)^2}\,d\xi \tag{2.12}$$

in which $\xi_{H'} = g\beta H'/kT$ where H', the total equivalent magnetic field exerted on the system, is defined as

$$H' = H + \frac{2K}{g\beta}\left(\frac{S_1+S_2+K/6J}{S_1-S_2}\right) \quad . \tag{2.13}$$

In evaluating the integral in (2.12), we first express $e^{\xi}(e^{\xi}-1)^{-2}$ as $\sum_{n=1}^{\infty} n e^{-n\xi}$ and then substitute $u = (\xi-\xi_{H'})^{1/2}$. The integral thus becomes

$$\sum_{n=1}^{\infty} 2n e^{-n\xi_{H'}} \int_0^{\infty} u^2(u^4 + 2\xi_{H'}u^2 + \xi_{H'}^2)\, e^{-nu^2}\,du \quad .$$

From tables,[8] we find that

$$\int_0^{\infty} x^{2a} e^{-\rho x^2}\,dx = \frac{1\cdot 3\cdot 5\ldots(2a-1)}{2^{a+1}\,p^a}\left(\frac{\pi}{p}\right)^{1/2} \tag{2.14}$$

and the integral is thus finally determined as

$$\frac{15\sqrt{\pi}}{8}\sum_{n=1}^{\infty}\left\{1 + \frac{4}{5}n\xi_{H'} + \frac{4}{15}(n\xi_{H'})^2\right\} n^{-5/2}\, e^{-n\xi_{H'}} \quad .$$

For the special case of $\xi_{H'} = 0$, this expression reduces to simply

$$\frac{15\sqrt{\pi}}{8}\sum_{n=1}^{\infty}{}' n^{-5/2} \quad \text{or} \quad \frac{15\sqrt{\pi}}{8}\zeta(5/2)$$

where the Riemann zeta function, $\zeta(5/2) = 1.341$. Consequently, the spin wave contribution to the specific heat of the ferrimagnetic system may be written as

$$\frac{(C_a)_{\xi_{H'}\neq 0}}{(C_a)_{\xi_{H'}=0}} = \frac{1}{1.341}\sum_{n=1}^{\infty}{}'\left\{1 + \frac{4}{5}n\xi_{H'} + \frac{4}{15}(n\xi_{H'})^2\right\} n^{-5/2}\, e^{-n\xi_{H'}} \qquad (2.15a)$$

and

$$(C_a)_{\xi_{H'}=0} = 0.113\, k\left\{\frac{(S_1-S_2)kT}{4JS_1S_2}\right\}^{3/2} . \qquad (2.15b)$$

If the anisotropy and applied magnetic fields are negligibly small, the specific heat follows a $T^{3/2}$ law exactly. However, should they be appreciable, (2.15a) indicates that the temperature dependence of the specific heat no longer follows such a simple relationship. In fact, from Figure 2a, where the right hand side of (2.15a) is shown as a function of $kT/g\beta H'$ (or $1/\xi_{H'}$), it is evident that at sufficiently low temperatures, any finite anisotropy or applied field will ultimately cause the temperature dependence of the specific heat to be exponential. To illustrate the change of the temperature dependence of the specific heat with applied field, we have plotted in Figure 2b the specific heat against absolute temperature for $g\beta H'/k=0$, 1, and 2 (i.e., for $H'= 0$, 7430, and 14860 gauss, if it assumed that $g = 2$). Finally, in Figure 3, we have plotted the right hand side of equation (2.15a) against $\xi_{H'}$ to show how the specific heat varies with applied field at constant temperature. The monotonic decrease of the specific heat with increasing H may be understood qualitatively from the fact that the spin excitational energies, $\hbar\omega$, increase with H (see equation (2.9)), thus contributing less to the specific heat.

If the zero-point energy is neglected for reasons analogous to those given by Anderson[2] for an antiferromagnetic system of large atomic spin, the total energy of our ferrimagnetic system may be written as

$$W = -6NJS_1S_2 - Ng\beta H(S_1-S_2)/2 + \sum_a n_a \tfrac{1}{2}h\omega$$

where n_a, a function of a, is the integral occupation number, and $N = 1/a^3$, the number of atoms per unit volume of the system. It follows that the partition function is

$$Z = \exp\left\{(12NJS_1S_2 + Ng\beta H(S_1-S_2))/2kT\right\} \prod_a (1 - e^{-\xi})^{-1} \quad .$$

Using this expression for Z together with (2.9), we determine the saturation magnetization as

$$M = kT \frac{\partial}{\partial H}(\ln Z) = Ng\beta(S_1-S_2)/2 - g\beta \sum_a (e^{\xi} - 1)^{-1} \quad .$$

Thus, M_o, the saturation magnetization at absolute zero, is $Ng\beta(S_1-S_2)/2$, and the variation of the relative saturation magnetization is found to be

$$\frac{M_o-M}{M_o} \text{ or } \frac{\Delta_o M}{M_o} = \frac{2}{N(S_1-S_2)} \sum_a (e^{\xi} - 1)^{-1} = \frac{2}{S_1-S_2} \int_{a=0}^{\infty} \frac{4\pi a^2 da}{e^{\xi} - 1} \quad . \qquad (2.16)$$

By means of (2.9), we convert (2.16) to

$$\frac{\Delta_o M}{M_o} = \frac{1}{2\pi^2(S_1-S_2)} \left\{\frac{(S_1-S_2)kT}{4JS_1S_2}\right\}^{3/2} \int_{\xi_{H'}}^{\infty} \frac{(\xi - \xi_{H'})^{1/2} d\xi}{e^{\xi} - 1} \quad . \qquad (2.17)$$

In determining the integral in (2.17), we first express $(e^{\xi} - 1)^{-1}$ as $\sum_{n=1}^{\infty} e^{-n\xi}$ and use the substitution, $u = (\xi - \xi_{H'})^{1/2}$. Then, by the application of (2.14), we get for this integral

$$(\sqrt{\pi}/2) \sum_{n=1}^{\infty} n^{-3/2} e^{-n\xi_{H'}}$$

which, for $\xi_{H'} = 0$, reduces to

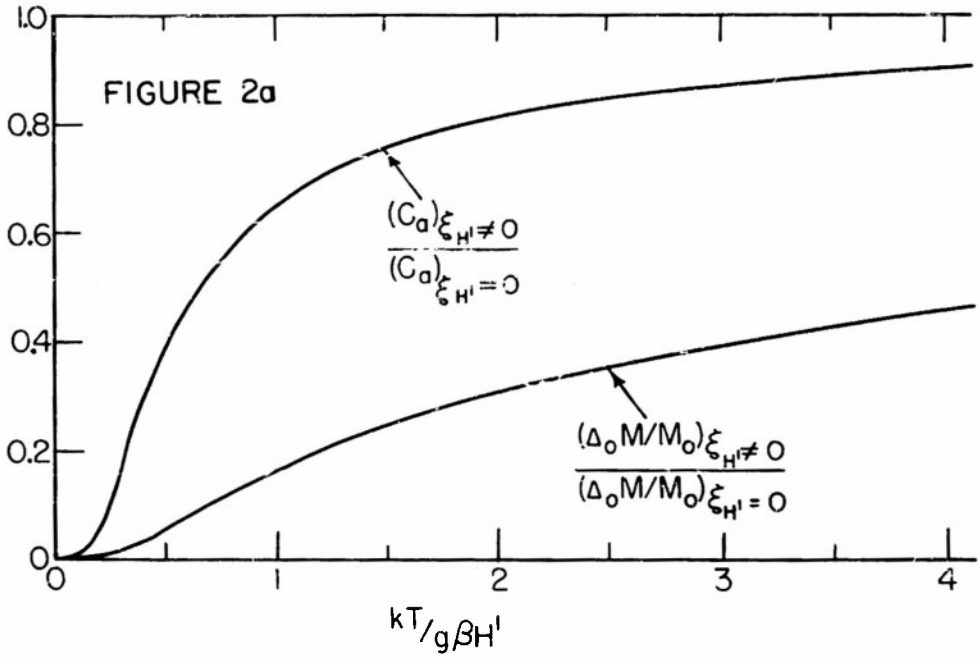
FIGURE 2a
1.0
0.8
0.6
0.4
0.2
0
0
1
2
3
4
$\frac{(C_a)_{\xi_{H'}\neq 0}}{(C_a)_{\xi_{H'}=0}}$
$\frac{(\Delta_0 M/M_0)_{\xi_{H'}\neq 0}}{(\Delta_0 M/M_0)_{\xi_{H'}=0}}$
$kT/g\beta H'$

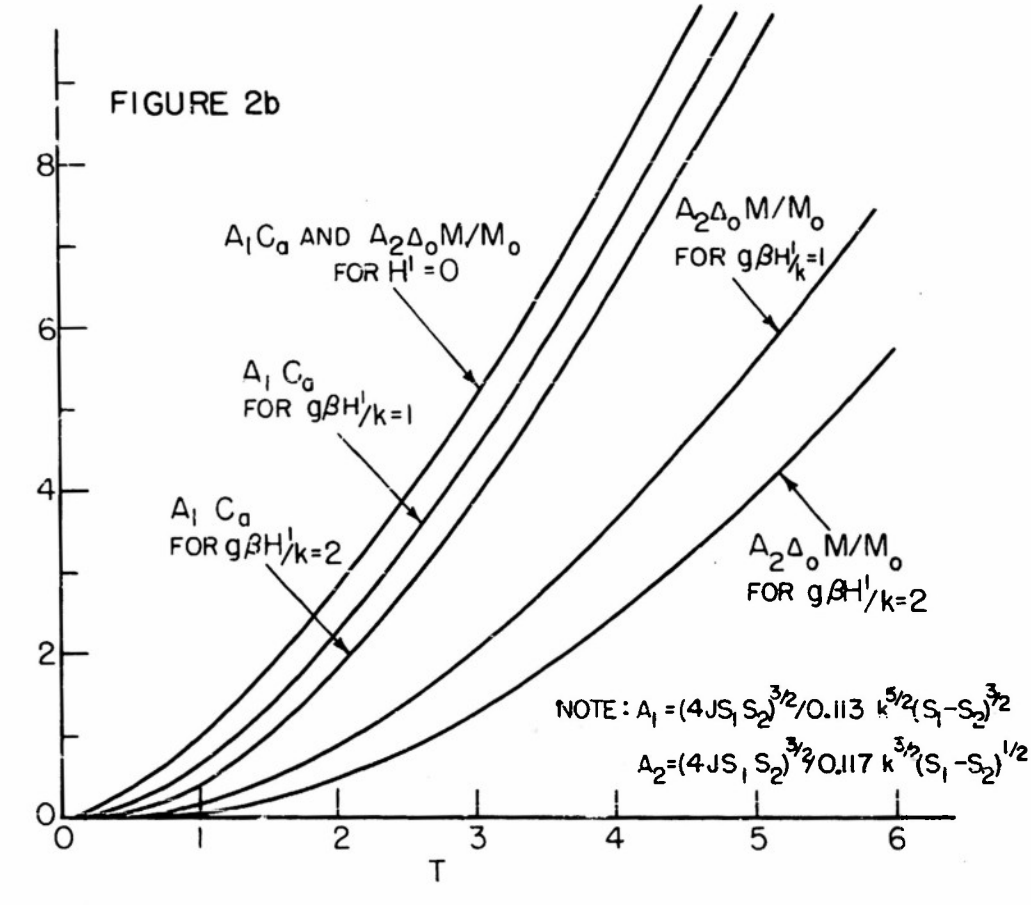
FIGURE 2b
8
6
4
2
0
0
1
2
3
4
5
6
T
$A_1 C_a$ AND $A_2\Delta_0 M/M_0$ FOR $H'=0$
$A_1 C_a$ FOR $g\beta H'/k=1$
$A_1 C_a$ FOR $g\beta H'/k=2$
$A_2\Delta_0 M/M_0$ FOR $g\beta H'/k=1$
$A_2\Delta_0 M/M_0$ FOR $g\beta H'/k=2$
NOTE: $A_1=(4JS_1S_2)^{3/2}/0.113\ k^{5/2}(S_1-S_2)^{3/2}$
$A_2=(4JS_1S_2)^{3/2}/0.117\ k^{3/2}(S_1-S_2)^{1/2}$

$$(\sqrt{\pi}/2)\,\zeta(3/2) \quad \text{or} \quad (\sqrt{\pi}/2)\,(2.612) \quad .$$

Hence, the relative saturation magnetization of the ferrimagnetic structure may be written as

$$\left(\frac{\Delta_o M}{M_o}\right)_{\xi_{H'}\neq 0} \Big/ \left(\frac{\Delta_o M}{M_o}\right)_{\xi_{H'}=0} = \frac{1}{2.612} \sum_{n=1}^{\infty}{}' n^{-3/2} e^{-n\xi_{H'}} \qquad (2.18a)$$

and

$$\left(\frac{\Delta_o M}{M_o}\right)_{\xi_{H'}=0} = \frac{0.117}{S_1 - S_2} \left\{\frac{(S_1 - S_2)kT}{4JS_1S_2}\right\}^{3/2} \quad . \qquad (2.18b)$$

Similar to the specific heat, $\Delta_o M/M_o$ departs from a $T^{3/2}$ law when the anisotropy and/or applied magnetic fields are sufficiently large. The approach to an essentially exponential temperature dependence of $\Delta_o M/M_o$ at low temperatures is shown in Figure 2a where the right hand side of equation (2.18a) has been plotted against $kT/g\beta H'$. In Figure 2b, $\Delta_o M/M_o$ has been plotted against absolute temperature for $g\beta H'/k = 0$, 1, and 2. It is quite evident that $\Delta_o M/M_o$ is much more strongly influenced than the specific heat by anisotropy and applied fields. This is also obvious from Figure 3 where the right hand side of equation (2.18a) has been plotted as a function of $\xi_{H'}$.

We previously showed that the expressions for the spin excitational energies for both the ferrimagnetic and ferromagnetic cases of the simple cubic model have the same form (see equations (2.9) and (2.10)). If we now go through the same procedure for the ferromagnetic case by starting with (2.10) instead of (2.9) and letting

$$H' = H + 2K/g\beta \quad , \qquad (2.19)$$

we find that equations (2.15a) and (2.18a) apply exactly, while (2.15b) and (2.18b) should be replaced by

$$(C_a)_{\xi_{H'}=0} = 0.113k\,(kT/2J'S)^{3/2} \qquad (2.20)$$

and

$$(\Delta_o M/M_o)_{\xi_{H'}=0} = (0.0587/S)\,(kT/2J'S)^{3/2} \qquad (2.21)$$

respectively. Equation (2.21) is in perfect agreement with Møller's[9] extension of Bloch's[10] original $T^{3/2}$ law, for the general case of $S \geq 1/2$; Mott and Jones[11] have obtained (2.20) for the case of $S = 1/2$.

Holstein and Primakoff[12] have investigated quantum mechanically the field dependence of the intrinsic magnetization of a ferromagnetic. If their magnetic dipole-dipole interaction terms are neglected, their expression that is analogous to equation (2.18a) but is valid only for small values of $\xi_{H'}$, may be written as

$$\left(\frac{\Delta_o M}{M_o}\right)_{\xi_{H'}\neq 0} \Big/ \left(\frac{\Delta_o M}{M_o}\right)_{\xi_{H'}=0} = 1 - 1.208\,\xi_{H'}^{1/2} \qquad (2.22)$$

and is represented in Figure 3 by the dashed curve. The agreement at low values of $\xi_{H'}$ with the curve corresponding to equation (2.18a) is very good. More important, perhaps, is the qualitative fact that both equations (2.18a) and (2.22) predict a sharp decrease of $\Delta_o M/M_o$ as $\xi_{H'}$ is increased from zero. It should be remembered, however, that $\xi_{H'}$ cannot be zero if the anisotropy of either the ferrimagnetic or ferromagnetic structure is not zero (see equations (2.13) and (2.19)).

3. The Antiferromagnetic Case

When $S_1 = S_2 = S$ in the spin structure shown in Figure 1 and the g-factors of the two sublattices are assumed equal, the net saturation magnetization of the system is zero. Hence, the system is antiferromagnetic. If we assume further that the anisotropy constants associated with the two sublattices are equal, the spin vibrational frequencies for this antiferromagnetic case are found directly from (2.7) to be

$$\hbar\omega = g\beta H \pm [4K(12JS + K) + (12JS)^2(4\pi^2 a^2/3)]^{1/2} \qquad (3.1)$$

when we also make use of (2.8). Consequently, in the absence of anisotropy and applied magnetic fields, ω is directly proportional to a. This particular dispersion law, as has already been pointed out by others,[2]

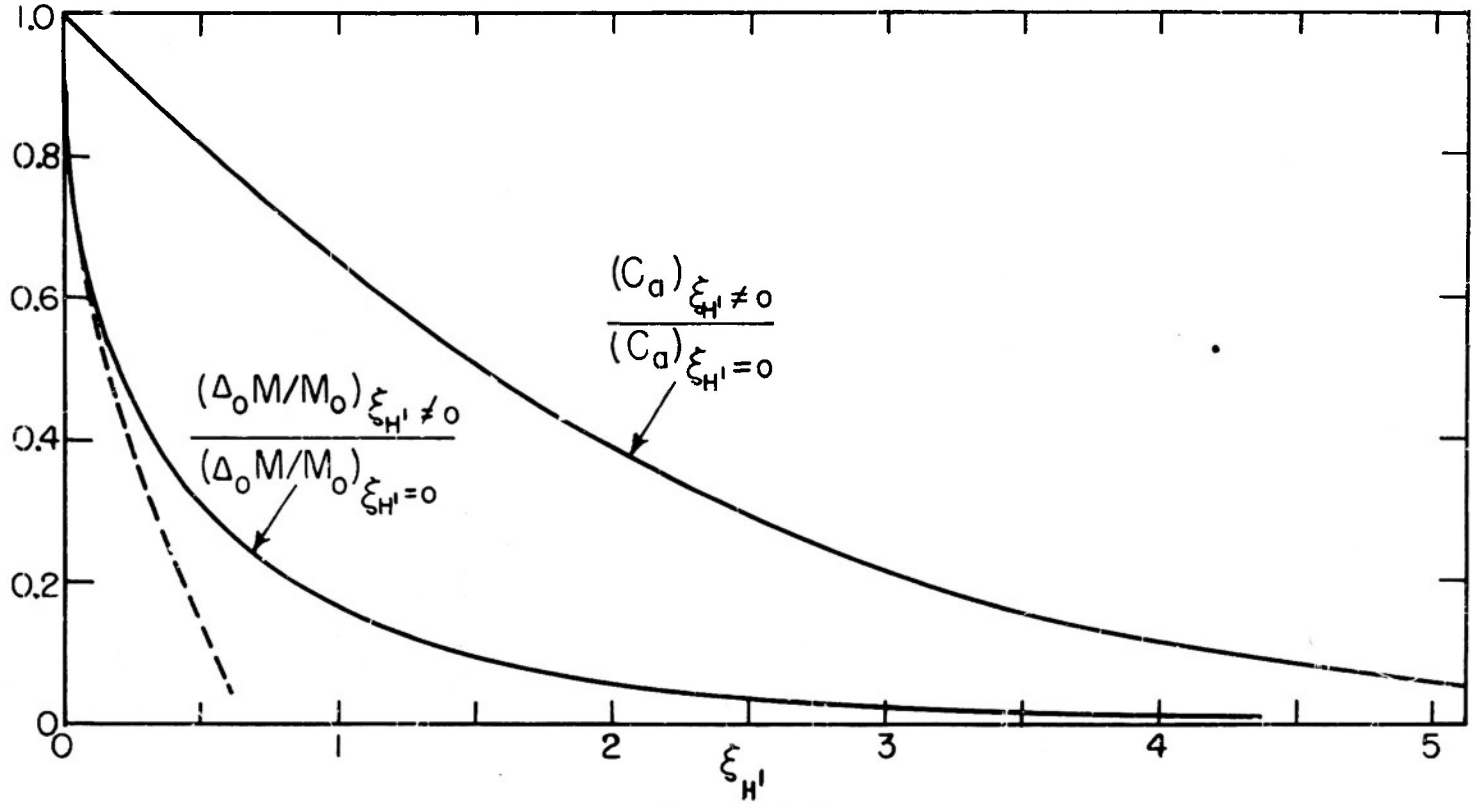
1.0
0.8
0.6
0.4
0.2
0
0
1
2
3
4
5
$\xi_{H'}$
$\frac{(C_a)_{\xi_{H'}\neq 0}}{(C_a)_{\xi_{H'}=0}}$
$\frac{(\Delta_0 M/M_0)_{\xi_{H'}\neq 0}}{(\Delta_0 M/M_0)_{\xi_{H'}=0}}$

FIGURE 3

gives rise to a T^3 variation of the specific heat (as compared to the $T^{3/2}$ variation in the ferrimagnetic and ferromagnetic cases).

The transition from (2.9) to (3.1) for the frequencies of spin vibration is a discontinuous one when S_1-S_2 is reduced from 1/2 to 0, if, as may be expected, S_1 and S_2 must have half-integral values in order that a spin wave analysis be valid. Hence, although the antiferromagnetic case represents an extreme case (i.e., when $S_1=S_2$) for the ferrimagnetic spin structure of Figure 1, far less similarity may be expected between the spin wave properties of an antiferromagnetic and a ferrimagnetic than between those of a ferrimagnetic and a ferromagnetic.

The existence of the two "acoustical" modes, corresponding to + and − in (3.1), was first pointed out by Kittel[13] in connection with antiferromagnetic resonance. Equation (3.1), itself, was derived more recently by Keffer et al.[14]

It will be shown later that there is a change of the spin state from that pictured in Figure 1 when $g\beta H$ exceeds $2[K(12JS-K)]^{1/2}$, which is smaller than $2[K(12JS+K)]^{1/2}$. Thus, the square root in (3.1), for the range of applied fields for which this equation is valid, will always be larger than $g\beta H$, and we should keep in mind that it is the absolute magnitude of ω which must be inserted in (2.11) to determine the specific heat. Let us write in place of (3.1),

$$\hbar|\omega| = [4K(12JS+K) + (12JS)^2 (4\pi^2 a^2/3)]^{1/2} \pm g\beta H \qquad (3.2)$$

Inserting (3.2) in (2.11), we obtain the following equation for the spinwave specific heat per atom:

$$C_a = \frac{(3)^{3/2} k}{2\pi^2} \left(\frac{kT}{12JS}\right)^3 \int_{\xi_o \mp \xi_H}^{\infty} G(\xi) \cdot (\xi \pm \xi_H) [(\xi \pm \xi_H)^2 - \xi_o^2]^{1/2} d\xi$$

$$G(\xi) = \xi^2 e^{\xi} (e^{\xi} - 1)^{-2} = [(\xi/2)/\sinh(\xi/2)]^2 = \sum_{n=1}^{\infty} n\xi^2 e^{-n\xi} \qquad (3.3)$$

where $\xi = \hbar|\omega|/kT$, $\xi_H = g\beta H/kT$, and $\xi_o = 2[K(12JS+K)]^{1/2}/kT$. For negligible

anisotropy and external fields (i.e., for ξ_o and $\xi_H \simeq 0$), the integral in (3.3) is readily evaluated by the use of the summation form of $G(\xi)$ and the tabulated integral[15]

$$\int_0^\infty x^b e^{-ax} dx = b!/a^{b+1} ,$$

and the final result for the specific heat is

$$(C_a)_{\xi_o+\xi_H=0} = \frac{(3)^{3/2} 4!\, \zeta(4)\, k}{2\pi^2} \left(\frac{kT}{12JS}\right)^3 \text{ times } 2$$

$$= 13.7\, k\, (kT/12JS)^3 . \qquad (3.4)$$

The multiplication by 2 is required to account for the two modes of spin vibration, which in this special case are degenerate. Thus, a simple T^3 law is followed. However, in the more general case of finite anisotropy (with or without an externally applied field), it is obvious that the specific heat deviates from a T^3 law by an amount determined by the integral in (3.3). Since we have been unable to evaluate this integral in its general form analytically in any simple manner, we have resorted to graphical integration.

Let us first examine the situation when there is a finite anisotropy but no applied magnetic field. In Figure 4a, the integrand of the integral in (3.3) has been plotted against ξ for various values of ξ_o. These curves were then integrated graphically; the results, multiplied by the coefficient shown in (3.3) (and by 2 to allow for the two degenerate modes of spin vibration), lead directly to the specific heat values shown plotted against ξ_o in Figure 4b. It is evident from this drawing that a finite magnetic anisotropy, especially since ξ_o depends roughly on the geometric mean of the anisotropy and exchange energies (the latter generally being by far the larger), would always cause a decrease of the specific heat. The lower the temperature, the more pronounced will be this effect. From Figure 5a where the specific heat normalized by its no-anisotropy value is shown as a function of $1/\xi_o$, we should note that at sufficiently low temperatures a finite anisotropy would result in an essentially exponential temperature

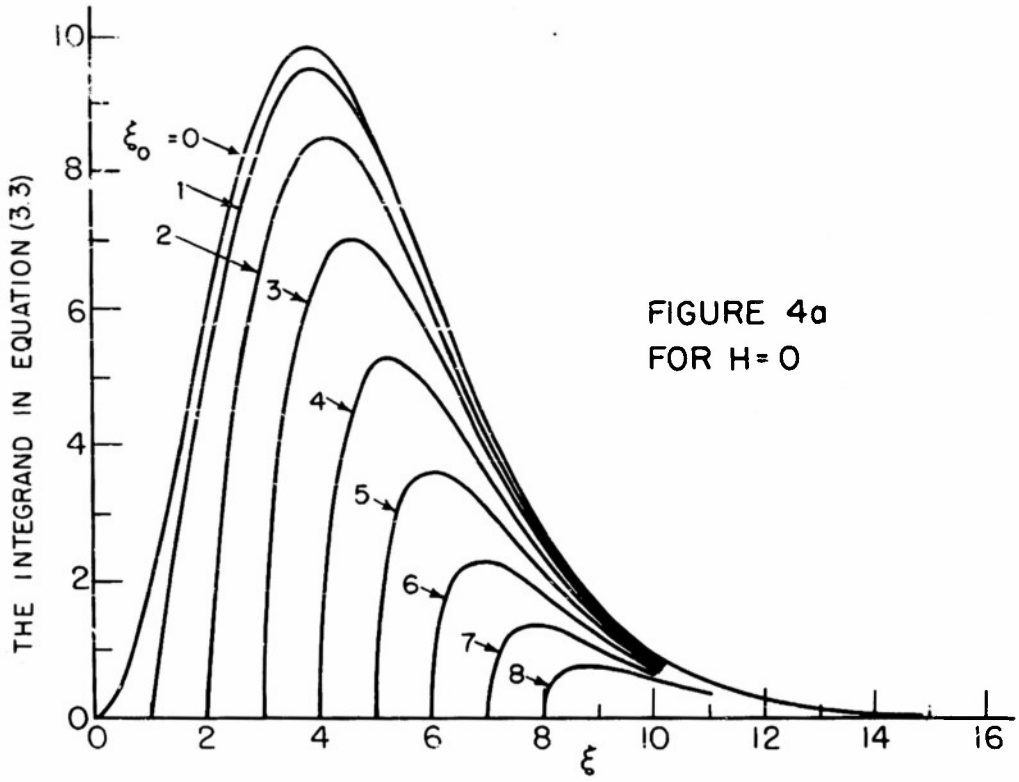

FIGURE 4a
FOR H = 0

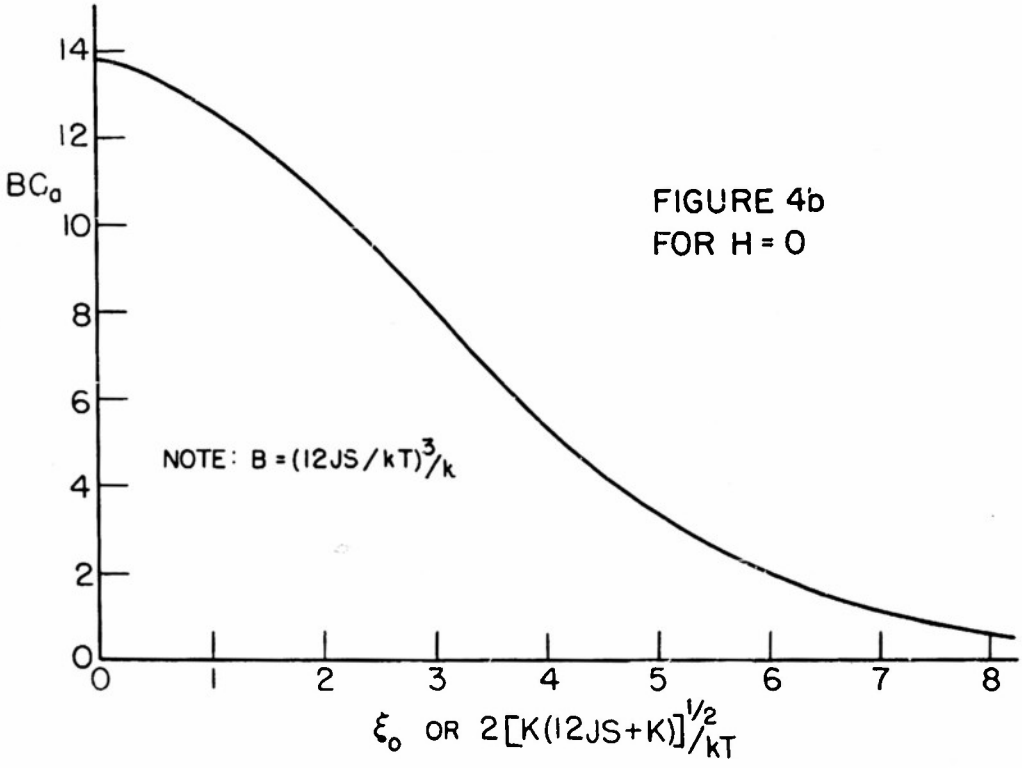

FIGURE 4b
FOR H = 0

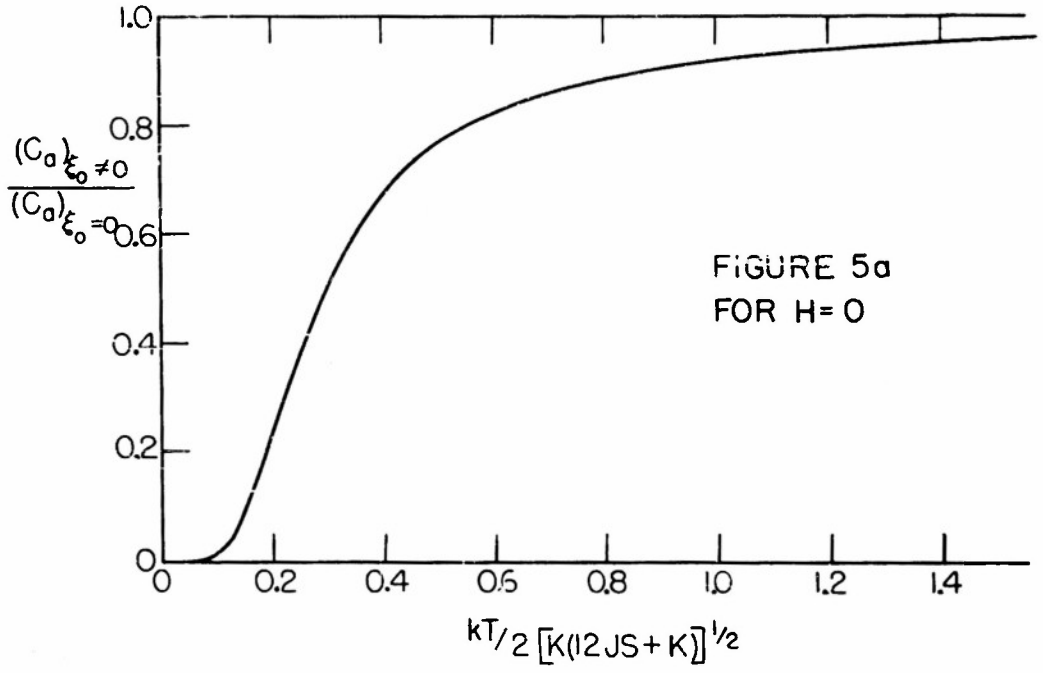

FIGURE 5a
FOR H = 0

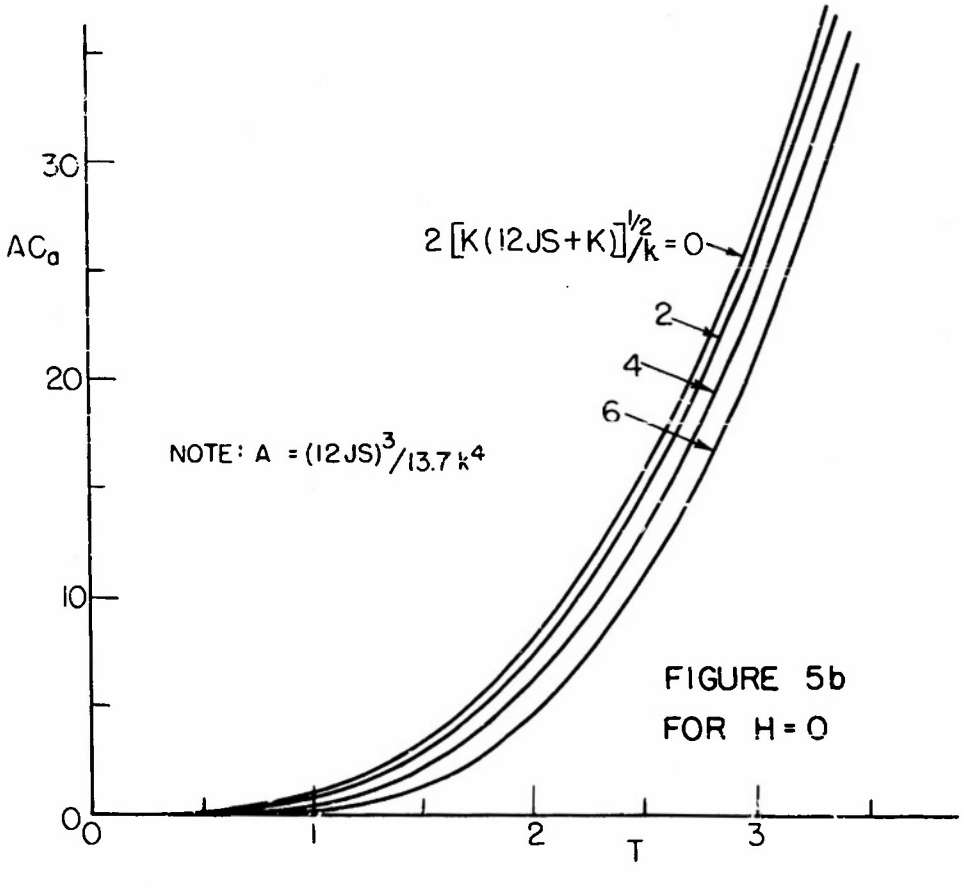

FIGURE 5b
FOR H = 0

dependence of the specific heat. Figure 5b may serve to illustrate more directly the effects of a finite magnetic anisotropy on the specific heat and its temperature dependence (i.e., the deviations from a pure T^3 law).

With the application of a magnetic field on the antiferromagnetic system, the degeneracy in the spin vibrational energies is removed (see equation (3.2)), and each of the two modes may be expected to contribute differently to the specific heat. As an example, we have set $\xi_o = 1$ and have plotted in Figure 6a the integrand in equation (3.3) against ξ for several values of ξ_H. For $\xi_H \neq 0$, the two parts of the integrand, corresponding to the lower energy (L.E.) mode and the higher energy (H.E.) mode, are both represented. Integrating these curves graphically, we obtain values for the specific heat which, in Figure 6b, have been plotted against ξ_H. It is clear from this figure that for an increase of the applied magnetic field, the increase of the contribution of the lower energy mode to the specific heat more than compensates for the decrease of the higher energy mode contribution. The net result is an increase of the spin wave specific heat of the antiferromagnetic system. This contrasts strongly with the ferrimagnetic and ferromagnetic cases for which the spin wave specific heat decreases monotonically for an increasing applied field (see Figure 3).

By a completely classical analysis of the ground state of the atomic spins of a simple cubic antiferromagnetic structure (discussed more fully in Appendix B), we have found that when the magnetic field applied along the anisotropy axis is raised above a certain critical value, an abrupt transition of the ground state spin configuration may be expected to take place. In Figure 7, we indicate schematically the arrangement of the atomic spin vectors of the two sublattices for State I, the original state of the system which we have been discussing, and for State II, the state when the applied field is higher than the critical value. It may be noted that in State II the spin vectors are not aligned antiparallel to each other, and hence give rise to a net magnetization. In addition, at the point of transition between states, there is a correspondingly abrupt change of the magnetic susceptibility parallel to the applied field, as Néel[16] was the first to point out.

Our primary interest here, however, in this transition of the spin state, is in its effects on the specific heat of the system. The spin wave problem for the spin configuration of State II must therefore be solved. As shown in Appendix B, the condition for which the transition between States I and II occurs, is

$$g\beta H = 2[K(12JS - K)]^{1/2} \quad , \tag{3.5}$$

and for State II, the angle θ, (see Figure 7) satisfies

$$\sin\theta = g\beta H/2(12JS - K) \quad . \tag{3.6}$$

Thus, if the field applied parallel to the anisotropy axis is increased beyond its value in (3.5), θ will increase monotonically until $g\beta H = 2(12JS - K)$, when the spins of both sublattices will have been brought into parallel alignment with each other and with H. However, since the magnitude of the exchange integral, J, of any antiferromagnetic crystal whose Curie point is above $4^{\circ}K$, is probably of the order of $(10)^{-16}$ ergs or more (see next section), it would not be possible in this case to achieve an appreciably large value of θ with any physically realizable magnetic field. Nevertheless, since it is fairly reasonable to expect that $K \ll 12JS$ for most antiferromagnetic crystals, it is still possible to achieve the applied fields required by (3.5) and even somewhat higher fields.

For the spin configuration of State II as shown in Figure 7, the equation of motion of a particular spin vector may be expressed by equation (2.1), but the rectangular components of the spin vectors must now be written as

$$\underline{S}^{(1)} = \hat{j}_x(S\cos\theta + S_x^{(1)}) + \hat{j}_y S_y^{(1)} + \hat{j}_z(S\sin\theta + S_z^{(1)}) \tag{3.7a}$$

$$\underline{S}^{(2)} = \hat{j}_x(-S\cos\theta + S_x^{(2)}) + \hat{j}_y S_y^{(2)} + \hat{j}_z(S\sin\theta + S_z^{(2)}) \quad , \tag{3.7b}$$

the dynamic components having their sublattice designated by superscripts. It is then assumed that the dynamic components have the spatial-wave form of (2.3). The resulting equations of motion for these components are:

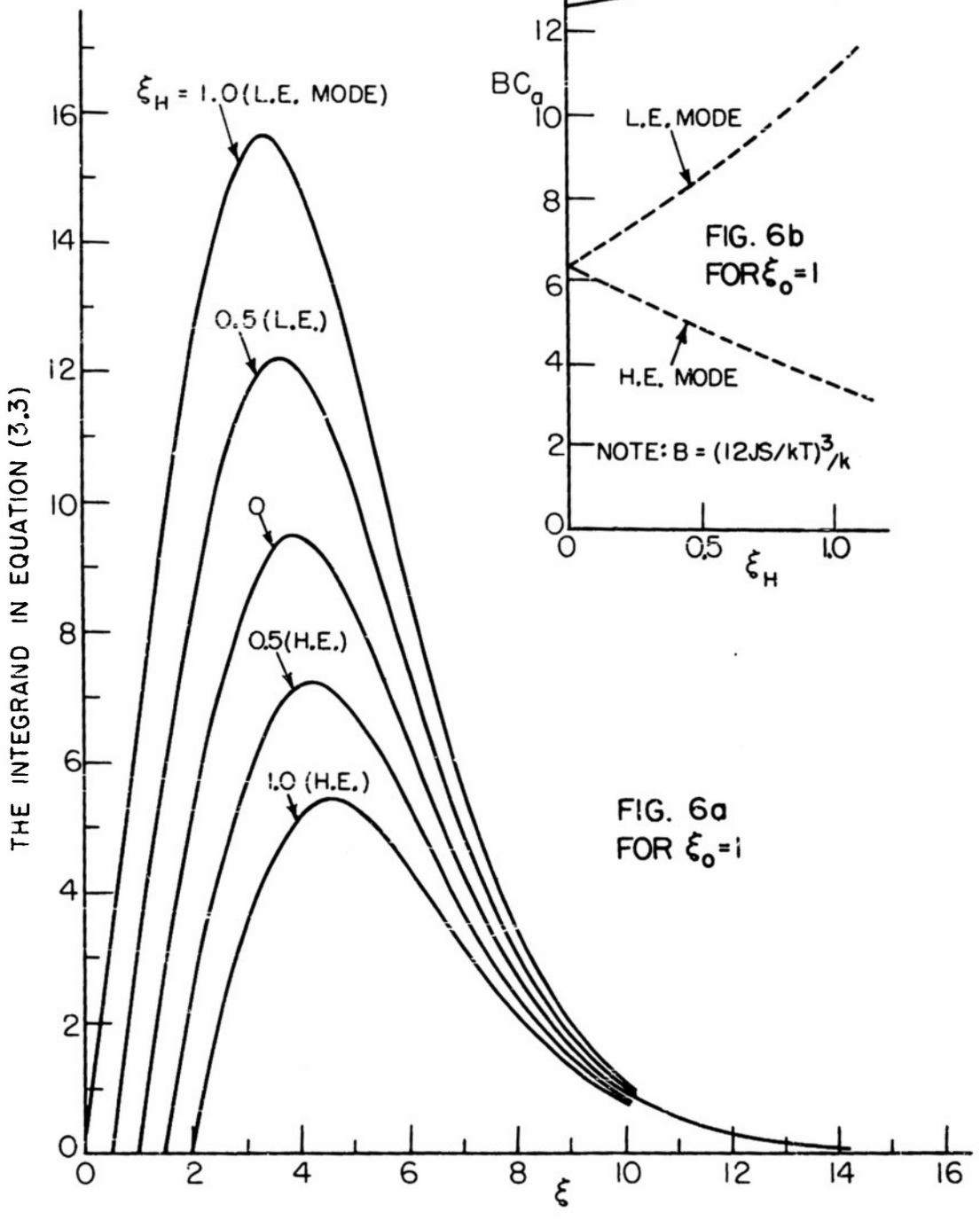

FIG. 6a
FOR $\xi_0 = 1$

FIG. 6b
FOR $\xi_0 = 1$

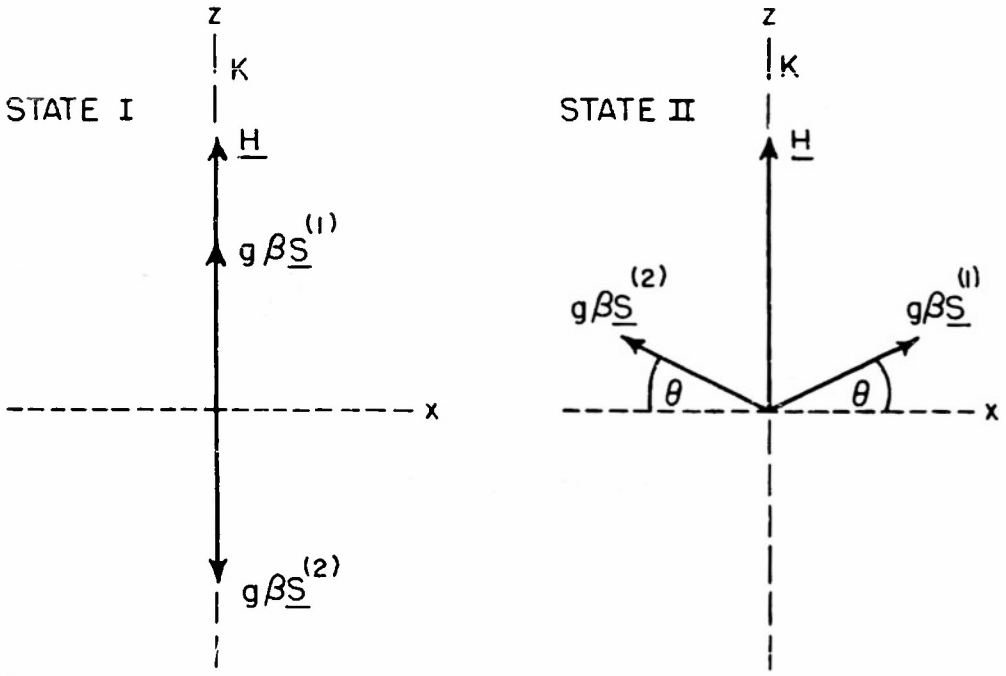

SPIN STATES FOR $\underline{H}$ II K-AXIS

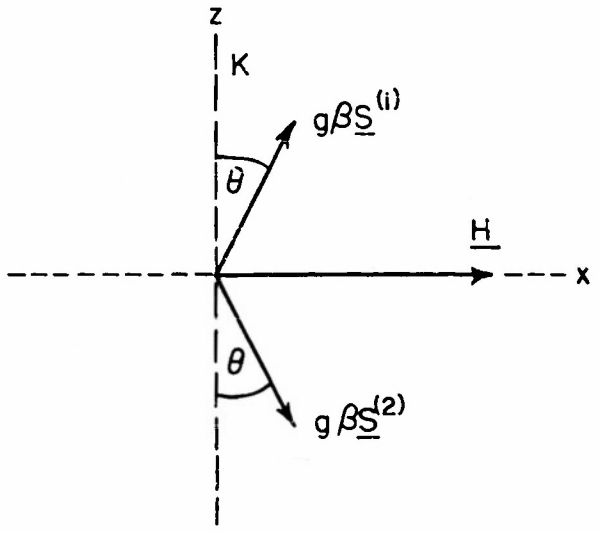

SPIN STATE FOR H ⊥ K-AXIS

FIGURE 7

$$\hbar\dot{S}_x^{(1)} = 12JS\gamma_a \sin\theta\, S_y^{(2)} - [(12JS - 2K)\sin\theta - g\beta H]S_y^{(1)} \qquad (3.8a)$$

$$\hbar\dot{S}_x^{(2)} = 12JS\gamma_a \sin\theta\, S_y^{(1)} - [(12JS - 2K)\sin\theta - g\beta H]S_y^{(2)} \qquad (3.8b)$$

$$\hbar\dot{S}_y^{(1)} = -12JS\gamma_a \sin\theta\, S_x^{(2)} + [(12JS - 2K)\sin\theta - g\beta H]S_x^{(1)} + 12JS\gamma_a \cos\theta S_z^{(2)} + (12JS - 2K)\cos\theta\, S_z^{(1)} \qquad (3.8c)$$

$$\hbar\dot{S}_y^{(2)} = -12JS\gamma_a \sin\theta\, S_x^{(1)} + [(12JS - 2K)\sin\theta - g\beta H]S_x^{(2)} - 12JS\gamma_a \cos\theta S_z^{(1)} - (12JS - 2K)\cos\theta\, S_z^{(2)} \qquad (3.8d)$$

$$\hbar\dot{S}_z^{(1)} = -12JS\gamma_a \cos\theta\, S_y^{(2)} - 12JS\cos\theta\, S_y^{(1)} \qquad (3.8e)$$

$$\hbar\dot{S}_z^{(2)} = 12JS\gamma_a \cos\theta\, S_y^{(1)} + 12JS\cos\theta\, S_y^{(2)} \qquad (3.8f)$$

when terms higher than the first order in the dynamic components are discarded. Since the spin vectors may be thought to oscillate about their static equilibrium positions defined by (3.6), no static (zero order) terms appear in the above equations. From a consideration of the time invariance of the spin vector magnitudes, it follows from (3.7) that the x and z dynamic spin components are interrelated by the equations,

$$-\frac{S_x^{(1)}}{\sin\theta} = \frac{S_z^{(1)}}{\cos\theta} = S_u^{(1)} \quad \text{and} \quad \frac{S_x^{(2)}}{\sin\theta} = \frac{S_z^{(2)}}{\cos\theta} = S_u^{(2)} \ ,$$

which also serve to define a new, convenient set of spin components, $S_u^{(1)}$ and $S_u^{(2)}$. Removing θ from equations (3.8) by means of (3.6), we find that in terms of the u and y spin components, equations (3.8a) and (3.8b) are identical with (3.3e) and (3.8f), respectively. The resultant four independent equations are

$$\hbar\dot{S}_u^{(1)} = -12JS\gamma_a S_y^{(2)} - 12JSS_y^{(1)} \qquad (3.9a)$$

$$\hbar\dot{S}_u^{(2)} = 12JS\gamma_a S_y^{(1)} + 12JSS_y^{(2)} \qquad (3.9b)$$

$$\hbar \dot{S}_y^{(1)} = 12JS\gamma_a (1 - R_H^2/2) S_u^{(2)} + [12JS - 2K(1 - R_H^2/4)] S_u^{(1)} \quad (3.9c)$$

$$\hbar \dot{S}_y^{(2)} = -12JS\gamma_a (1 - R_H^2/2) S_u^{(1)} - [12JS - 2K(1 - R_H^2/4)] S_u^{(2)} \quad (3.9d)$$

where $R_H = g\beta H/(12JS - K)$. Assuming each dynamic spin component varies harmonically with time (i.e., as $e^{\pm i\omega t}$), we proceed to combine (3.9a) with (3.9b), and (3.9c) with (3.9d) to form two pairs of linear equations, one in $S_u^{(1)} - S_u^{(2)}$ and $S_y^{(1)} + S_y^{(2)}$, and the other in $S_u^{(1)} + S_u^{(2)}$ and $S_y^{(1)} - S_y^{(2)}$. The solutions for the two modes of spin vibrational frequencies are then found from these equations to be

$$\hbar^2\omega^2 = (12JS)^2 (1 - R_H^2/2)(1 - \gamma_a^2) + (12JS)^2 (R_H^2/2)(1 \pm \gamma_a) - 24JSK(1 - R_H^2/4)(1 \pm \gamma_a) \quad . \quad (3.10)$$

We now make use again of the low temperature approximation for γ_a (i.e., equation (2.8)); thus, we find for the choice of the negative sign and the positive sign in (3.10) that the frequencies for the two modes of State II may be written as

$$\hbar^2\omega^2 = (12JS)^2 \left(1 - \frac{K}{12JS}\right)\left\{1 - \frac{(g\beta H)^2}{4(12JS - K)^2}\right\}\left(\frac{4\pi^2}{3} a^2\right) \quad (3.11)$$

and

$$\hbar^2\omega^2 = 48JSK\left\{\left(\frac{12JS}{K} + 1\right)\frac{(g\beta H)^2}{4(12JS - K)^2} - 1\right\} + (12JS)^2\left\{1 + \frac{K}{12JS} - \left(3 + \frac{K}{12JS}\right)\frac{(g\beta H)^2}{4(12JS - K)^2}\right\}\left(\frac{4\pi^2}{3} a^2\right), \quad (3.12)$$

respectively. It may be readily seen that the forms of these equations are special cases of the more general form of equation (3.2). Hence, the contribution of the mode represented by (3.11) to the specific heat may be expressed as a T^3 relationship (similar to (3.4)), while the specific heat due to the mode represented by (3.12) must be expressed in a more complicated form (similar to (3.3) with $\xi_H = 0$). For a numerical example of the variation of the specific heat with applied field at a constant temperature, we have chosen the conditions, 12JS/kT = 15 and K/12JS = 0.00111. Thus, $\xi_o = 1$, for which we already have computed the specific heat for State I (as indicated in Figure 6b); furthermore, the transition between States I and II will occur when the condition, $\xi_H = 2[K(12JS - K)]^{1/2}/kT = 0.999$ is satisfied. Calculating the specific heat contributions of the two modes of State II, represented by equations (3.11) and (3.12), we find that with increasing applied field, the former rises very slowly while the latter decreases relatively quickly. The net effect is a decrease of the total specific heat of the system. The calculated results are shown in Figure 8, and it is quite evident that there is a distinct difference between States I and II in the manner in which the spin wave specific heat varies with a magnetic field applied along the anisotropy axis. We should also note that at the point of transition between States I and II, there is an abrupt discontinuity in the total specific heat of the antiferromagnetic system.

Let us turn now to the situation in which a magnetic field is applied perpendicular to the anisotropy axis (and along one of the other cube edges) of the simple cubic antiferromagnetic system. In this case, as shown in Appendix B, there is only one possible static equilibrium spin state within the applied field range of interest (as compared to the two for the case just previously discussed). The corresponding spin configuration of the two sublattice system is represented schematically in Figure 7. It is fairly obvious, incidentally, that this configuration also represents the only stable spin state of a simple cubic antiferromagnetic structure having cubic anisotropy, when a small field is applied along one of the three mutually-perpendicular anisotropy axes. With reference to this figure, the angle, θ, satisfies the condition

$$\sin\theta = g\beta H/2(12JS + K) \quad , \tag{3.13}$$

and, thus, as the applied field is increased from zero, θ increases monotonically to $\pi/2$. However, for reasons previously mentioned, only small values of θ may be expected to be physically attainable, and our subsequent calculations of the spin wave specific heat will be restricted, therefore, to this region of applied fields.

The starting point of the spin wave problem is once again the equation of motion (2.1). The rectangular components of the spin vectors of the two sublattices may now be expressed as

$$\underline{S}^{(1)} = \hat{j}_x(S\sin\theta + S_x^{(1)}) + \hat{j}_y S_y^{(1)} + \hat{j}_z(S\cos\theta + S_z^{(1)}) \tag{3.14a}$$

$$\underline{S}^{(2)} = \hat{j}_x(S\sin\theta + S_x^{(2)}) + \hat{j}_y S_y^{(2)} + \hat{j}_z(-S\cos\theta + S_z^{(2)}) \quad . \tag{3.14b}$$

The applied field is taken to be in the x direction. Again assuming that the dynamic spin components have the spatial-wave form of (2.3), we find that the first order equations of motion of these components are

$$\hbar\dot{S}_x^{(1)} = 12JS\gamma_a\cos\theta\, S_y^{(2)} + (12JS+2K)\cos\theta\, S_y^{(1)} \tag{3.15a}$$

$$\hbar\dot{S}_x^{(2)} = -12JS\gamma_a\cos\theta\, S_y^{(1)} - (12JS+2K)\cos\theta\, S_y^{(2)} \tag{3.15b}$$

$$\hbar\dot{S}_y^{(1)} = -12JS\gamma_a\cos\theta\, S_x^{(2)} - (12JS+2K)\cos\theta\, S_x^{(1)} + 12JS\gamma_a\sin\theta\, S_z^{(2)} - [(12JS+2K)\sin\theta - g\beta H]\, S_z^{(1)} \tag{3.15c}$$

$$\hbar\dot{S}_y^{(2)} = 12JS\gamma_a\cos\theta\, S_x^{(1)} + (12JS+2K)\cos\theta\, S_x^{(2)} + 12JS\gamma_a\sin\theta\, S_z^{(1)} - [(12JS+2K)\sin\theta - g\beta H]\, S_z^{(2)} \tag{3.15d}$$

$$\hbar\dot{S}_z^{(1)} = -12JS\gamma_a\sin\theta\, S_y^{(2)} + [12JS\sin\theta - g\beta H]\, S_y^{(1)} \tag{3.15e}$$

$$\hbar\dot{S}_z^{(2)} = -12JS\gamma_a\sin\theta\, S_y^{(1)} + [12JS\sin\theta - g\beta H]\, S_y^{(2)} \quad . \tag{3.15f}$$

Since the magnitudes of the spin vectors are time independent, it may be deduced from equations (3.14) that

$$\frac{S_x^{(1)}}{\cos\theta} = \frac{-S_z^{(1)}}{\sin\theta} = S_v^{(1)} \quad \text{and} \quad \frac{S_x^{(2)}}{\cos\theta} = \frac{S_z^{(2)}}{\sin\theta} = S_v^{(2)} \quad .$$

Making use of (3.13) to remove θ from equations (3.15), we find that in terms of the y and the newly defined v components of spin, equations (3.15) reduce to the four independent equations,

$$\hbar\dot{S}_v^{(1)} = 12JS\gamma_a S_y^{(2)} + (12JS + 2K)\, S_y^{(1)} \tag{3.16a}$$

$$\hbar\dot{S}_v^{(2)} = -12JS\gamma_a S_y^{(1)} - (12JS + 2K) S_y^{(2)} \tag{3.16b}$$

$$\hbar\dot{S}_y^{(1)} = -12JS\gamma_a(1 - Q_H^2/2)\, S_v^{(2)} - [12JS + 2K(1 - Q_H^2/4)]\, S_v^{(1)} \tag{3.16c}$$

$$\hbar\dot{S}_y^{(2)} = 12JS\gamma_a(1 - Q_H^2/2) S_v^{(1)} + [12JS + 2K(1 - Q_H^2/4)] S_v^{(2)} \tag{3.16d}$$

where $Q_H = g\beta H/(12JS+K)$. The dynamic spin components are assumed to vary harmonically with time; thus, it becomes possible to combine (3.16a) with (3.16b), and (3.16c) with (3.16d) to form one pair of linear equations in $S_v^{(1)} - S_v^{(2)}$ and $S_y^{(1)} + S_y^{(2)}$ and an other in $S_v^{(1)} + S_v^{(2)}$ and $S_y^{(1)} - S_y^{(2)}$. The two modes of spin variational frequencies, corresponding to the solutions of these two pairs of equations, are found to be

$$\hbar^2\omega^2 = 4K(12JS + K)(1 - Q_H^2/4) + (12JS)^2 (1 - Q_H^2/2)(1 - \gamma_a^2) + 12JS(12JS + K)(Q_H^2/2)(1 \pm \gamma_a) \tag{3.17}$$

which, upon use of (2.8) as the low temperature approximation for γ_a, is converted to

$$\hbar^2\omega^2 = 4K(12JS+K)\left\{1 - \frac{(g\beta H)^2}{4(12JS+K)^2}\right\}$$

$$+(12JS)^2\left\{1 - (1 - \frac{K}{12JS})\ \frac{(g\beta H)^2}{4(12JS+K)^2}\right\}\left(\frac{4\pi^2}{3}\ a^2\right) \qquad (3.18)$$

and

$$\hbar^2\omega^2 = 4K(12JS+K)\left\{(\frac{12JS}{K} - 1)\ \frac{(g\beta H)^2}{4(12JS+K)^2} + 1\right\}$$

$$+(12JS)^2\left\{1 - (3 + \frac{K}{12JS})\ \frac{(g\beta H)^2}{4(12JS+K)^2}\right\}\left(\frac{4\pi^2}{3}\ a^2\right), \qquad (3.19)$$

corresponding respectively to - and + in (3.17). In the absence of an applied field, both (3.18) and (3.19) reduce properly to (3.2) in which H has been set to zero. The two modes thus become degenerate. From the forms of (3.18) and (3.19), it follows that the spin wave contribution of each mode to the specific heat may be represented by an expression that is similar to (3.3) with $\xi_H = 0$. For comparison with our previous calculations, we have chosen the conditions, 12JS/kT = 15 and K/12JS = 0.00111, for which to work out a numerical example of the dependence of the specific heat (at a fixed temperature) on the magnetic field applied perpendicular to the anisotropy axis. The calculated results are shown in Figure 9, from which it is evident that for an increase of the applied field, the rise of the specific heat contribution of the mode represented by (3.18) is more than compensated by the decrease of that of the mode represented by (3.19). The net result is a decrease of the total specific heat.

It would be interesting to examine together the effects on the total spin wave specific heat, of a magnetic field applied parallel to the anisotropy axis and of a field applied perpendicular to this axis. Consequently, in Figure 10, we have superimposed the pertinent curves, which appear separately in Figures 8 and 9, for the conditions, 12JS/kT = 15 and K/12JS = 0.00111. Moreover, we have calculated the same types of curves for the same value of 12JS/kT but for K/12JS = 0.00444. These

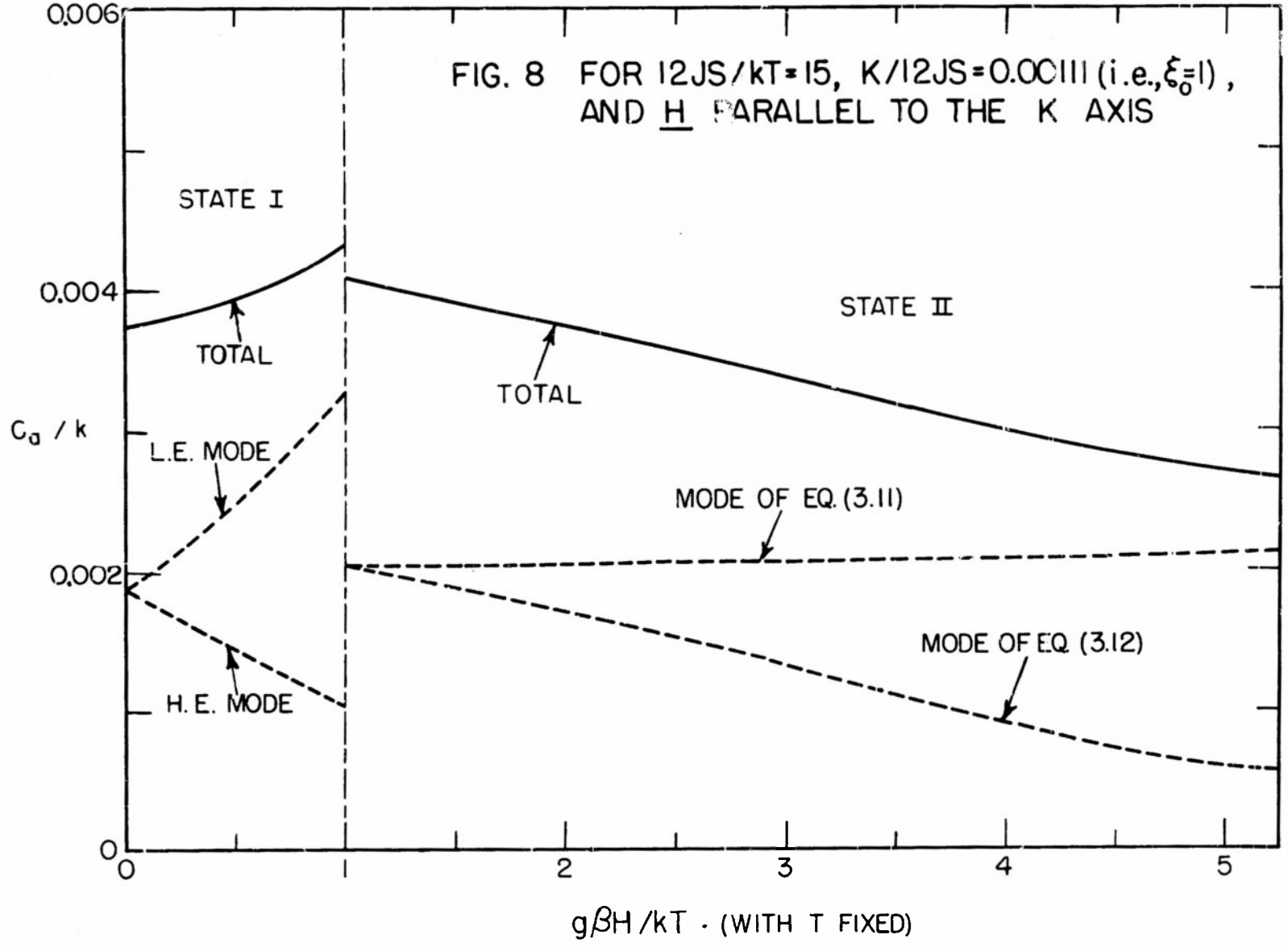
FIG. 8 FOR 12JS/kT=15, K/12JS=0.00111 (i.e., ξ_0=1), AND H PARALLEL TO THE K AXIS
0.006
0.004
0.002
0
C_a / k
STATE I
STATE II
TOTAL
TOTAL
L.E. MODE
MODE OF EQ. (3.11)
MODE OF EQ. (3.12)
H. E. MODE
0
2
3
4
5
$g\beta H/kT$ · (WITH T FIXED)

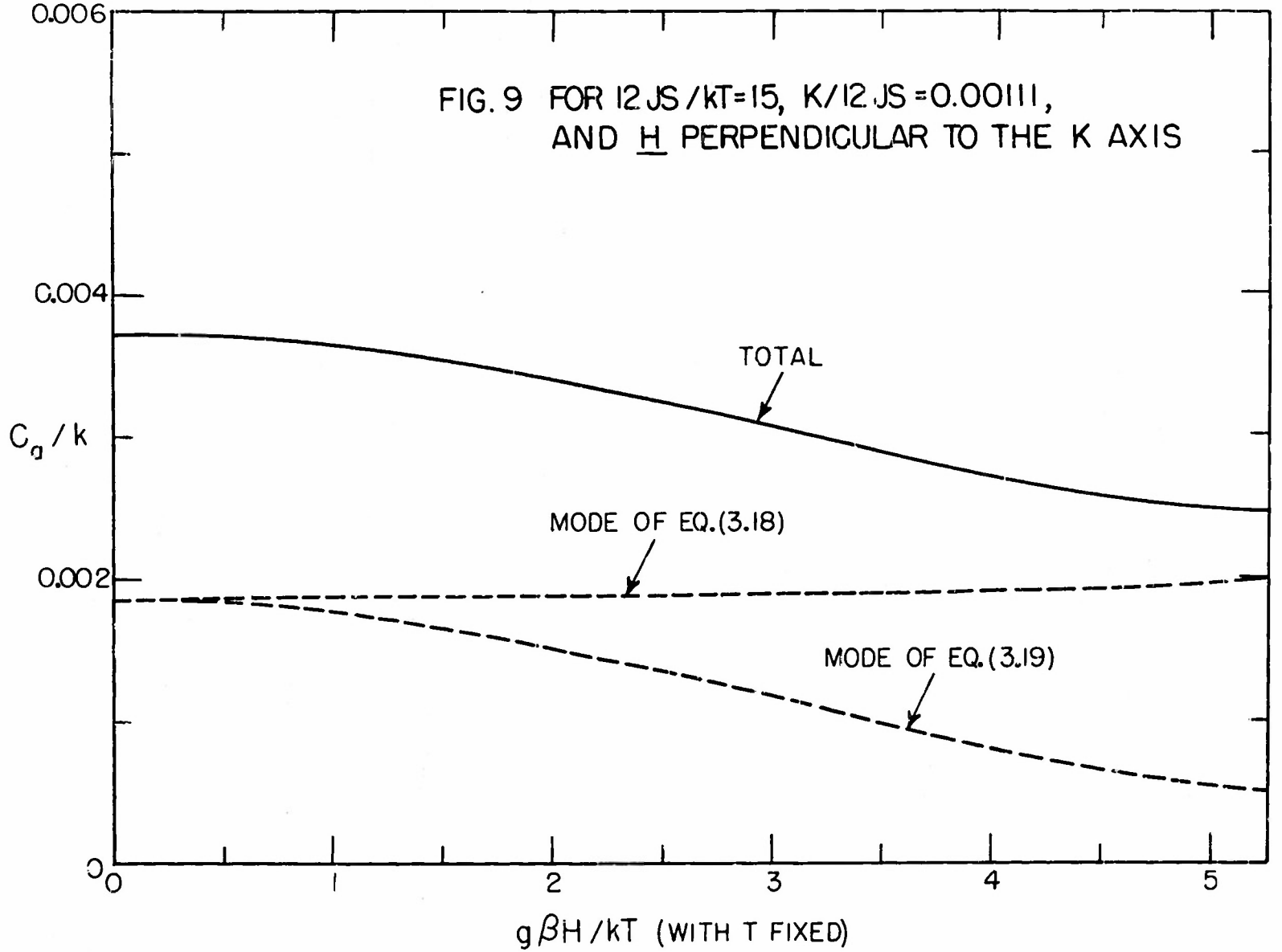

FIG. 9 FOR $12JS/kT = 15$, $K/12JS = 0.00111$, AND $\underline{H}$ PERPENDICULAR TO THE K AXIS

curves, also, are shown in Figure 10. It becomes evident that the abrupt change of specific heat that accompanies the transition between States I and II (for H parallel to the K-axis) is greater, the larger the magnetic anisotropy. Furthermore, beyond these transitions of spin state (i.e., for higher applied fields), a larger anisotropy causes a bigger difference between the specific heat when the applied field is parallel to the anisotropy axis, and the specific heat when the field is perpendicular to this axis.

If the magnetic anisotropy is considered to be negligibly small, both equations (3.11) and (3.18) reduce to

$$\hbar^2\omega^2 = [(12JS)^2 - (g\beta H/2)^2]\ (4\pi^2 a^2/3) \quad , \tag{3.20}$$

and both (3.12) and (3.19) become equal to

$$\hbar^2\omega^2 = (g\beta H)^2 + [(12JS)^2 - 3(g\beta H/2)^2]\ (4\pi^2 a^2/3) \quad . \tag{3.21}$$

Hence, these equations represent the two modes of spin vibration for a magnetically isotropic simple cubic antiferromagnetic system with a magnetic field applied along a cube edge. It follows from previous discussion that the specific heat due to the mode represented by (3.20) will follow a simple T^3 law, while the temperature dependence of the specific heat due to the mode represented by (3.21) will have a more complicated behavior (described by an equation similar to (3.3) with $\zeta_H = 0$). Although this isotropic case may not have much physical significance, it does provide an interesting extreme case for which the field dependence of the specific heat may be compared to that of the system with a finite magnetic anisotropy. Therefore, once again for 12JS/kT = 15, we have calculated the specific heat contributions of the modes represented by (3.20) and (3.21), and we have found that for an increase of the applied field (at a fixed temperature), the decrease of the latter more than compensates for the increase of the former. The resultant decrease of the total specific heat is quite clear from Figure 10, in which the total specific heat of this isotropic case has been plotted over the applied field range of interest.

4. Comparison with Experiment

Since the preceding spin wave analyses were developed semiclassically and the determinations of the ground state spin configurations were purely classical, we certainly cannot rely rigorously on our theoretical results for quantitative comparison with experiment. Nevertheless, these results could be taken seriously, were it possible to examine them with reference to any thermal or magnetic measurements conducted at low temperatures (where, presumably, the spin wave theory is valid) on a ferrimagnetic or antiferromagnetic material having a simple cubic structure. Unfortunately, while there have been numerous such measurements on ferromagnetic metals and alloys, only a few studies have been made of the low temperature spin wave properties of a ferrimagnetic or antiferromagnetic structure of any type of crystalline symmetry. This is particularly true if we disregard recent spin resonance experiments, which are not of direct interest in this report. Hence, we are left with only the possibility of making some qualitative predictions about any experiments that are suggested by our simple theory, using any existing and pertinent experimental information for starting points of discussion.

To date, the main experimental evidence for the existence of a $T^{3/2}$ law has been the temperature dependence of the saturation magnetization of ferromagnetic metals at low temperatures.[17] It is significant, perhaps, that the decrease of the magnetization of gadolinium was found to be proportional to $T^{3/2}$ all the way up to its Curie point, while the magnetizations of nickel and iron at intermediate temperatures follow a T^2 relationship (which is explained by Stoner[18] on a collective electron theory basis). We shall refer to this later.

Of several papers on measurements of the temperature dependence of the magnetization of various ferrites,[19] the most recent one by Pauthenet, containing considerable tabulated data, is the most suitable for the present discussion. Unfortunately, except for a few low temperature points used to establish the magnetizations at absolute zero, all his measurements (on several simple ferrites and a family of mixed ferrites) were made above room temperature. Nevertheless, we shall attempt here a crude comparison

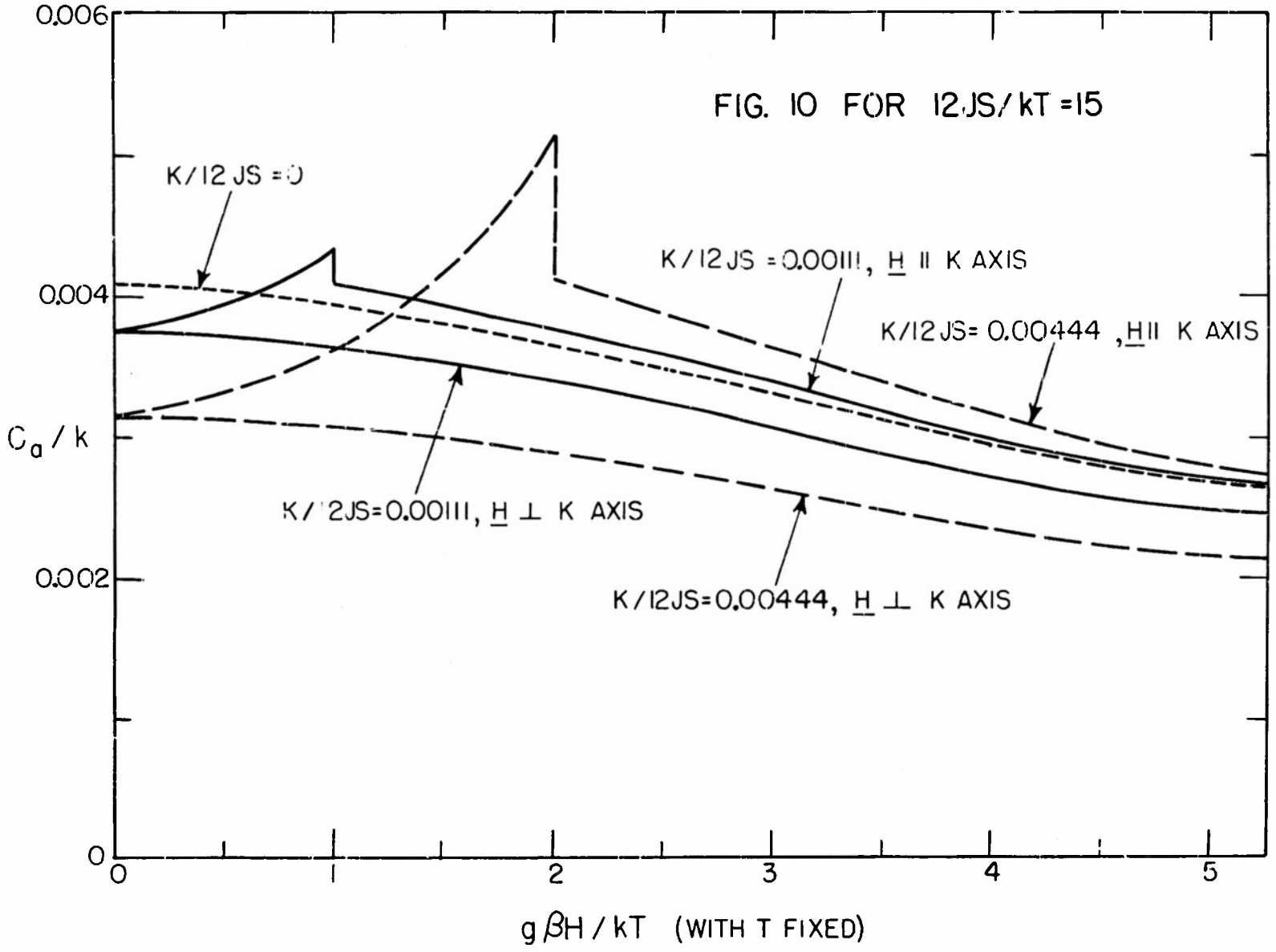
FIG. 10 FOR 12JS/kT =15
K/12JS =0
K/12JS =0.00111, H II K AXIS
K/12JS= 0.00444 ,H II K AXIS
K/12JS=0.00111, H ⊥ K AXIS
K/12JS=0.00444, H ⊥ K AXIS
0.006
0.004
0.002
0
C_a / k
0
1
2
3
4
5
$g\beta H / kT$ (WITH T FIXED)

between these measurements and the predictions of our simple spin wave theory. Equation (2.18b) is the relevant expression, if the effects of magnetic anisotropy and large applied fields are to be neglected. The octohedral (B) and the tetrahedral (A) sites in the actual ferrite structure[20] will be considered roughly equivalent to the atom sites in sublattices (1) and (2), respectively, of our simple cubic system; thus, effectively, the spins of the atoms of the two B sites of each unit cell will be coupled rigidly together. Hence, for the simple ferrites, we set $S_2 = 2.5$ (i.e., the spin of one ferric ion), and $S_1 = S_T + 2.5$, where S_T is the experimentally determined average magnetic moment per atom divided by 2β. For the mixed nickel-zinc ferrites (i.e., $(NiO)_{1-x}(ZnO)_x Fe_2O_3$), we shall allow for the apparent substitution of non-magnetic zinc ions for ferric ions in the A sites and the transfer of these ferric ions (with reversed spin) to the B sites, by setting $S_2 = 2.5\,(1-x)$ and $S_1 = S_T + 2.5(1-x)$. This can be only even approximately valid for $x \leq 0.5$ since the magnetic moment per ferrite molecule actually decreases for larger values of x.

Let us now find a relationship between the exchange integral in (2.18b) and the Curie temperature, T_c. According to the modern version of the Weiss field theory,[21] we may write for the z components (i.e., those in the direction of the applied field) of the magnetizations of the two sublattices:

$$M_z^{(1)} = Ng\beta S_z^{(1)} = Ng\beta S_1 \cdot B_{S_1}\left(12JS_1S_z^{(2)}/kT\right)$$

$$M_z^{(2)} = Ng\beta S_z^{(2)} = Ng\beta S_2 \cdot B_{S_2}\left(12JS_2S_z^{(1)}/kT\right) \quad . \qquad (4.1)$$

Remembering that the Brillouin function, $B_S(u) \simeq (S+1)u/3S$ for $u \ll 1$, we obtain from (4.1) two linear equations in $S_z^{(1)}$ and $S_z^{(2)}$, whose compatibility condition fixes T_c as follows:

$$kT_c = 4J\left[S_1S_2(S_1+1)(S_2+1)\right]^{1/2} \quad . \qquad (4.2)$$

Consequently, (2.18b) may be rewritten as

$$\Delta_o M/M_o = A_M (T/T_c)^{3/2}$$

$$A_M = 0.117 (S_1 - S_2)^{1/2} [(S_1+1)(S_2+1)/S_1 S_2]^{3/4} \qquad (4.3)$$

when anisotropy and applied field effects are neglected.

Starting with Pauthenet's values for T_c and S_T, we have calculated S_1, S_2, J, and A_M for our simple cubic models for the simple ferrites of nickel, cobalt, iron, and manganese, and for various mixed nickel-zinc ferrites. The results are listed in Table 1. Furthermore, we have converted Pauthenet's data into equivalent A_M versus T/T_c points, which are shown in Figure 11. The solid curves through these points have been restricted to the temperature range over which we believe the experimental points are dependable. The values of A_M which we previously calculated and listed in Table 1, are represented in Figure 11 by the horizontal long-dashed lines.

By a different manipulation of his data, Pauthenet was able to conclude that $\Delta_o M/M_o$ at low temperatures for nickel, cobalt, and iron ferrites followed a T^2 law, while that of manganese ferrite varied as $T^{3/2}$. The short dashed lines in Figure 11 correspond quantitatively to these temperature variations. However, from this figure, it appears to us that for all four simple ferrites, as well as for the mixed ferrites, it is quite likely that the limiting values of A_M, as $T \rightarrow 0$, are other than zero. If they should approach their limiting values along a horizontal tangent in Figure 11, the $T^{3/2}$ law for low temperatures would be confirmed. Moreover, as in the cases of metallic iron and nickel, the temperature dependence of $\Delta_o M/M_o$ for nickel, cobalt and iron ferrites probably shifts gradually from $T^{3/2}$ to T^2, as the temperature is increased from a very low value. The relative magnetization of manganese ferrite, however, like that of metallic gadolinium, probably follows a $T^{3/2}$ law over the entire ferrimagnetic temperature range. Our calculated low temperature values of A_M are all undoubtedly too low. However, particularly for the mixed ferrites, their relative magnitudes appear to be in the right sequence. This is as much as could be expected in view of the drastic approximation made in fitting the actual ferrites into "equivalent" simple cubic models. A spin wave

Table I

$YO \cdot Fe_2O_3$							
Y	S_T	S_1	S_2	$T_c(^oK)$	J/k	A_M	$C \cdot T^{-\frac{3}{2}}$ $\frac{\text{millijoules}}{^oK - \text{mole}}$ $(^oK)^{-\frac{3}{2}}$
Ni	1.11	3.61	2.50	870	18.0	0.190	0.132
Co	1.97	4.47	2.50	769	13.1	0.245	0.366
Fe	2.04	4.54	2.50	847	14.3	0.250	0.332
Mn	2.20	4.70	2.50	576	9.4	0.258	0.660

$(NiO)_{1-x}(ZnO)_x \cdot Fe_2O_3$							
X	S_T	S_1	S_2	$T_c(^oK)$	J/k	A_M	$C \cdot T^{-\frac{3}{2}}$ $\frac{\text{millijoules}}{^oK - \text{mole}}$ $(^oK)^{-\frac{3}{2}}$
0.1	1.51	3.76	2.25	814	17.8	0.226	0.250
0.2	1.89	3.89	2.00	755	17.7	0.259	0.378
0.3	2.24	3.99	1.75	671	17.1	0.290	0.600
0.4	2.48	3.98	1.50	618	17.9	0.320	0.830
0.5	2.72	3.97	1.25	548	18.4	0.355	1.206

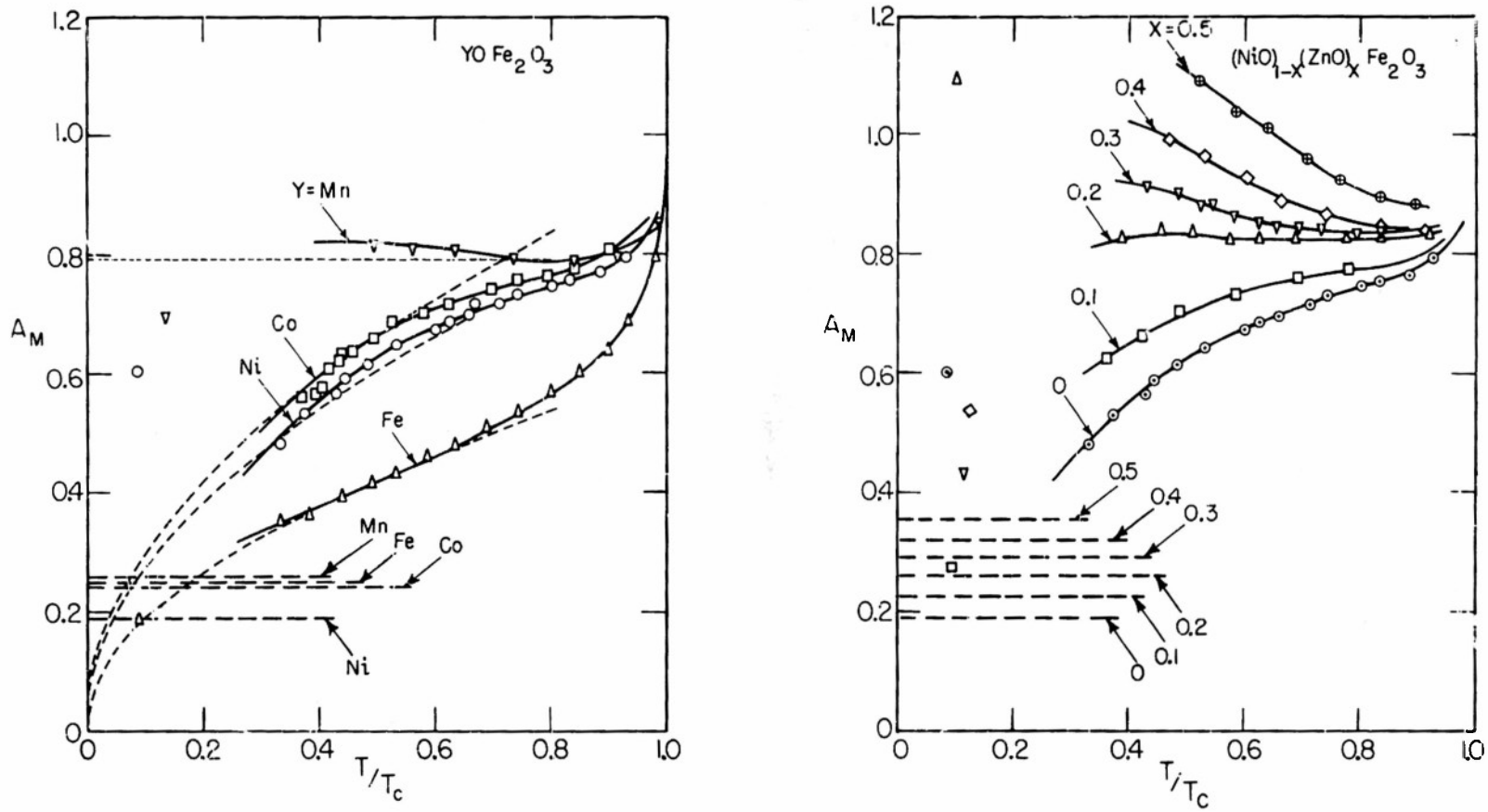
YO Fe2 O3
Y=Mn
Co
Ni
Fe
Mn
Fe
Co
Ni
AM
T/Tc
X=0.5
(NiO)1-X(ZnO)X Fe2 O3
0.4
0.3
0.2
0.1
0
0.5
0.4
0.3
0.2
0.1
0
AM
T/Tc

FIGURE 11

analysis more appropriate for the spinel structures of the ferrites, should make more dependable calculations possible; we propose to study this problem in the near future.

Needless to say, accurate low temperature measurements of the saturation magnetizations of the various ferrites are badly needed. The accuracy required to determine the temperature dependence of $\Delta_o M/M_o$ unambiguously, however, is extremely difficult to attain at low temperatures where a very small change of a very large quantity must be measured. Here, we suspect, lies the main advantage of low temperature measurements of the spin wave contribution to the specific heat. Another advantage of specific heat measurements over those of magnetization is the fact that any appreciable magnetic anisotropy of the ferrimagnetic structure may be expected to have a greater effect on the temperature variation of magnetization than on that of the specific heat (see Figure 3). The large applied fields required for the magnetic measurements would tend to aggravate this situation. Hence, the experimental results for the temperature dependence of the specific heat can probably be more easily interpreted in terms of the coefficient of a simple $T^{3/2}$ relationship (see equation (2.15b)), than can the results for the temperature dependence of magnetization.

In many ferromagnetic metals and alloys whose low temperature specific heats have been measured, the electronic specific heat due to the energy band structure of the d electrons, has been large enough to mask any possible spin wave contribution. We have found, however, that the spin wave specific heat of a ferrimagnetic simple cubic structure also follows a $T^{3/2}$ law (see equations (2.15)) and is thus experimentally distinguishable from that due to lattice vibrations (which, of course, is proportional to T^3 at low temperatures). It seems reasonable to assume that this is true for ferrimagnetic materials of any crystalline structure. Hence, the ferrites, whose electronic specific heats are probably very small, appear to be the obvious materials for spin wave specific heat measurements.

Using (2.15b) and (4.2), we have calculated the spin wave specific heats for the different ferrites discussed previously. The resulting specific heat values, which have been listed in Table 1, are per mole,

where the molecule has been taken to consist of two adjacent lattice sites of the simple cubic model. Note the comparatively high spin wave specific heats of the mixed ferrites that have relatively low Curie temperatures (but whose exchange integrals, incidentally, are not very different from those of the simple ferrites). However, it is the magnitude of the spin wave specific heat relative to that of the lattice specific heat, that is of prime experimental importance. About the only specific heat measurements on any of the ferrites, to date, have been those of Millar[22] on iron ferrite (magnetite) down to liquid air temperatures. Assuming that at very low temperatures, the Debye temperature of iron ferrite is about the same (i.e., about 565°K) as at higher temperatures, we find that the spin wave and lattice vibration contributions to the specific heat are both equal at 2.7°K to about 1.5 millijoules/°K mol. At temperatures higher than 2.7°K, the lattice specific heat will predominate. Hence, the specific heat measurements should be carried out down to liquid helium temperatures. The low specific heat will necessitate extreme care in the calorimetry. An interesting supplementary experiment at these temperatures, preferably on a single crystal ferrite specimen, would be the measurement of the dependence of the spin wave specific heat on the strength of an applied magnetic field.

If the effects of anisotropy and applied fields are ignored, the spin wave specific heat of a simple cubic antiferromagnetic structure has been shown in Section 3 to be proportional to T^3. Thus, it would not be easily separable experimentally from the lattice specific heat at low temperatures, unless the spin wave contribution were very large due to the small magnitude of the exchange interaction integral (see equation (3.4)). The Curie or Néel temperature for the antiferromagnetic structure may be expressed by (4.2) if we set $S_1 = S_2 = S$; the equation then becomes simply

$$kT_c = 4JS(S+1) \quad . \qquad (4.4)$$

Hence, it follows that spin wave specific heat measurements should be possible with antiferromagnetic materials having low Curie temperatures (and low electronic specific heats).

Specific heat measurements were recently completed by Friedberg[23] on cupric chloride. Up to the Curie temperature (about 4.3°K), the total specific heat of this antiferromagnetic compound was found to be over one hundred times as large as the estimated lattice specific heat and was roughly proportional to T^3. However, since these measurements were made down to only 1.5°K, it is almost certain that the anomolously large specific heat, as well as its cubic temperature dependence, are associated primarily with an order-disorder transformation of the spin state, rather than with small perturbations of an ordered spin state. Hence, to determine the normal spin wave specific heat of cupric chloride, it would be necessary to extend these measurements down to temperatures in the region of $T_c/10$ (i.e., about 0.5°K) and study the variation of the specific heat over a very restricted temperature range.

Although most other antiferromagnetic salts have higher Curie points, we find, when we substitute (4.4) in (3.4) and obtain

$$C_a = 0.507\ k(S+1)^3\ (T/T_c)^3 \quad , \qquad (4.5)$$

that a larger electronic spin of the magnetic ions would tend to counterbalance the effect of a higher Curie point on the magnitude of the spin wave specific heat. Let us, therefore, make a rough estimate of the spin wave specific heat of ferrous chloride, whose Curie point is about 24°K, by assuming that the spin associated with each lattice site of our simple cubic model is 2 (i.e., the spin of one ferrous ion). We substitute this value of S into equation (4.5) and obtain for the spin wave specific heat: $8.2\ T^3$ millijoules/$(°K)^4$ mole, (a molecule is considered equivalent to one lattice site of the simple cubic model). Let us then suppose that the lattice specific heat of ferrous chloride is not very different from that of cupric chloride (i.e., about $1.1\ T^3$ millijoules/$(°K)^4$ mole). Hence, the spin wave specific heat, due to its large relative magnitude, should be quite separable from the lattice specific heat. Furthermore, we find from (4.4) that J = k, and if we assume that $K \simeq 0.1\ k$, it follows that $2[K(12JS+K)]^{1/2} \simeq 3.1\ k$. Thus, with reference to Figures 5a and 5b, it appears that for the temperatures at which the specific heat measurements on ferrous chloride should be carried out (i.e., in the region of

$T_c/10$ or 2.4°K), the spin wave specific heat should be well out of the exponential temperature dependence region.

Magnetic measurements on single crystals of manganese flouride[24] and cupric chloride[25] have confirmed Neel's prediction that a transition of spin state occurs when a magnetic field applied along the anisotropy axis of an antiferromagnetic crystal, attains a certain critical value. It would be most interesting, therefore, to make the accompanying specific heat measurements and learn if the magnetic field dependence of the spin wave contribution can be represented by a curve similar to that in Figure 8. For the sake of comparison, these specific heat measurements should also be made with the field applied perpendicular to the anisotropy axis (see Figure 10).

Acknowledgment

The authors wish to thank Professor N. Bloembergen for his constructive criticism of the manuscript of this report.

Appendix A

The Effects of Next-to-Nearest Neighbor Exchange Interactions

In the simple cubic atomic spin structure shown in Figure 1, each atom has twelve next-to-nearest neighbors, all of which lie on the same spin sublattice. To be consistent with the current theory on the properties of ferrites,[3] we assume that the next-to-nearest neighbor exchange interactions for both sublattices are negative, similar to but considerably weaker than the nearest neighbor interactions. Hence, the net electronic spins of nearest neighbor atoms are still mutually antiparallel, although the net exchange force on each spin is somewhat smaller than it would be in the absence of next-to-nearest neighbor interactions. We may expect, therefore, that the introduction of negative next-to-nearest neighbor interactions into our analysis will result in an increase of the spin wave specific heat of the system. It may be of interest, however, to examine their effects more quantitatively.

We let $-J_1$ and $-J_2$ be the exchange integrals for the next-to-nearest neighbor interactions between spins on sublattices (1) and (2), respectively. As before, $-J$ is the exchange integral for the nearest neighbor interactions. Thus, J_1, J_2, and J are all positive quantities. Furthermore, $J \gg J_1$ or J_2. If we now assume that the equation of motion of a particular spin vector has the form of (2.1), and then use (2.2) and (2.3), we find that the equations of motion for the spin components are the same as (2.4) except that to (a), (b), (c), and (d) must be added: $-24J_1S_1(1-\gamma'_a)S_y^{(1)}$, $+24J_2S_2(1-\gamma'_a)S_y^{(2)}$, $+24J_1S_1(1-\gamma'_a)S_x^{(1)}$, and $-24J_2S_2(1-\gamma'_a)S_x^{(2)}$, respectively, where $\gamma'_a = (\cos 2\pi a_x \cos 2\pi a_y + \cos 2\pi a_y \cos 2\pi a_z + \cos 2\pi a_z \cos 2\pi a_x)/3$. When (2.5a) is used, this is equivalent to adding $-24J_1S_1(1-\gamma'_a)S_+^{(1)}$ and $+24J_2S_2(1-\gamma'_a)S_+^{(2)}$ to (2.6a) and (2.6b), respectively. Thus, again setting $g_1 = g_2 = g$ and $K_1 = K_2 = K$, we obtain for the spin wave frequencies:

$$\hbar\omega = g\beta H - 6J(S_1 - S_2) - 12(J_1S_1 - J_2S_2)(1 - \gamma'_a)$$

$$\pm \Big[\{6J(S_1 - S_2) + 12(J_1S_1 - J_2S_2)(1 - \gamma'_a)\}^2 + (12J)^2 S_1S_2(1 - \gamma_a^2)$$

$$+ 2K\{12J(S_1 + S_2) + 2K - 24(J_1S_1 + J_2S_2)(1 - \gamma'_a)\}$$

$$- 24(J_1S_1^2 + J_2S_2^2)(12J)(1 - \gamma'_a)$$

$$+ (24J_1S_1)(24J_2S_2)(1 - \gamma'_a)^2 \Big]^{1/2}. \qquad \text{(A. 1)}$$

For spin waves of very long wavelength, a is very small, and, therefore, $1 - \gamma'_a \simeq 4\pi^2a^2/3$, which is also the small-a value of $1 - \gamma_a^2$.

In the ferrimagnetic case, $6J(S_1 - S_2)$ may be expected to be by far the the dominant term in (A. 1); hence, the plus sign must be chosen for the "acoustical" mode. Furthermore, we can now expand the square root in (A. 1) binomially, and, neglecting higher order terms in a, we get

$$\hbar\omega \simeq g\beta H + 2K\left\{\frac{S_1 + S_2 + K/6J}{S_1 - S_2}\right\} \qquad \text{(A. 2)}$$

$$+ \frac{12}{S_1 - S_2}\left[JS_1S_2 - 2J_1S_1\left\{S_1 + \frac{K}{6J}\right\} - 2J_2S_2\left\{S_2 + \frac{K}{6J}\right\}\right](4\pi^2a^2/3).$$

A comparison of (A. 2) with (2. 9) reveals that the only effect of next-to-nearest neighbors interactions on the expression for ω is a decrease of the coefficient of a^2. It can be easily shown that, correspondingly, both the specific heat and the temperature variation of the magnetization are increased by a factor equal to the 3/2 power of the ratio of the coefficient of a^2 in (2.9) to that in (A.2). The dependences of C_a and $\Delta_o M/M_o$ on the applied magnetic field, however, are still described by (2.15a) and (2.18a), respectively.

For the antiferromagnetic case, we set $S_1 = S_2 = S$ and $J_1 = J_2$; as a result, we find from (A.1) that the expression analogous to (3.2) may be written as

$$\hbar|\omega| = \left[4K(12JS+K)+(12JS)^2\left\{1-\frac{4J_1}{J}\left(1+\frac{K}{6JS}\right)\right\}\left(\frac{4\pi^2}{3}a^2\right)\right]^{1/2} \pm g\beta H \qquad (A.3)$$

It follows that the introduction of next-to-nearest neighbor exchange interactions causes an increase of the specific heat of the antiferromagnetic system by the factor $\left\{1 - 4J_1(1 + K/6JS)/J\right\}^{-3/2}$. As in the ferrimagnetic case, the field dependence of the specific heat is not changed by these additional interactions.

Since all next-to-nearest neighbor atoms in our simple cubic model lie in the same sublattice, their electronic spin vectors have parallel ground-state orientations whether the system is in State I or in State II (see Figure 7). Hence, the criterion for the transition of the antiferromagnetic system from one spin state to the other is not affected by next-to-nearest neighbor interactions.

Appendix B

The Static Equilibrium States of the Antiferromagnetic Spin System

It will be assumed that the electronic spin vectors of the simple cubic atomic system are subjected only to forces arising from negative exchange interactions between nearest neighbor spins and from interactions with a magnetic anisotropy field and a uniform applied magnetic field. The corresponding energies will be expressed as the purely classical equivalents of the energy terms in equation (2.1). The g-factors as well as the anisotropy constants associated with the two sublattices will be considered equal.

We are interested in determining the static equilibrium positions of the spin vectors, first, when the applied field is parallel to the anisotropy axis. It is fairly obvious in this case that the spin vectors must lie in planes that are parallel to each other and to the anisotropy axis. The problem, therefore, may be formulated with reference to the schematic two-dimensional vector diagram of Figure 12, in which the orientations of two nearest neighbor spin vectors are defined by the angles, χ and θ. The energy of the system of N atoms may be written then as

$$E = -6NJS^2\cos 2\theta - \tfrac{1}{2}Ng\beta HS[\cos(\chi - \theta) + \cos(\pi - \chi - \theta)]$$

$$+ \tfrac{1}{2}NKS[\sin^2(\chi - \theta) + \sin^2(\pi - \chi - \theta)]$$

or $$E/NS = 6JS(2\sin^2\theta - 1) - g\beta H \sin\theta \sin\chi$$

$$+ K(\sin^2\theta + \sin^2\chi - 2\sin^2\theta \sin^2\chi). \qquad (B.1)$$

It is easily established that as long as $K \leq 6JS$ (which is certain to be satisfied in practice), the value of θ that minimizes (B.1) may be expressed by

$$\sin\theta = \frac{(g\beta H/2)\sin\chi}{12JS + K(1 - 2\sin^2\chi)}, \qquad (B.2)$$

for which (B.1) becomes

$$E/NS = -6JS + K\sin^2\chi - \frac{(g\beta H/2)^2 \sin^2\chi}{12JS + K(1 - 2\sin^2\chi)}. \qquad (B.3)$$

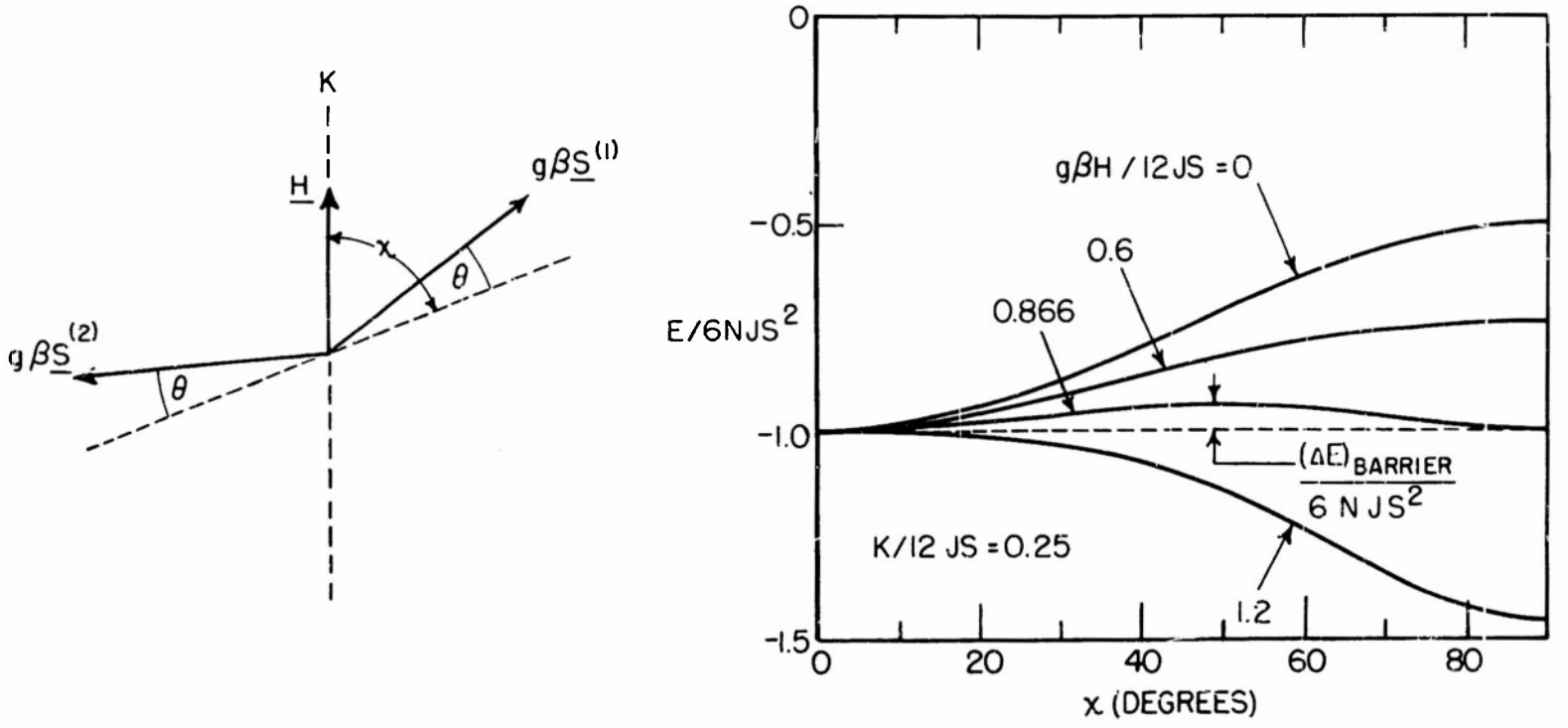
K
H
gβS(1)
gβS(2)
θ
θ
χ
0
-0.5
-1.0
-1.5
E/6NJS2
gβH / 12JS = 0
0.6
0.866
1.2
(ΔE)BARRIER / 6 N J S2
K/12 JS = 0.25
0
20
40
60
80
χ (DEGREES)

FIGURE 12

It is then found that with respect to χ , (B.3) has stationary values for

$$\sin \chi = 0, \quad \sin\theta = 0; \tag{B.4a}$$

$$\sin \chi = 1, \quad \sin\theta = g\beta H/2(12JS - K); \tag{B.4b}$$

and $$\sin^2\chi = \frac{12JS + K}{2K}\left[1 - \frac{(g\beta H/2)}{[K(12JS + K)]^{1/2}}\right] = \frac{12JS + K}{K}\sin^2\theta, \tag{B.4c}$$

for which the corresponding energies are respectively,

$$E/NS = -6JS, \tag{B.5a}$$

$$E/NS = -6JS + K - (g\beta H/2)^2/(12JS - K), \tag{B.5b}$$

and $$E/NS = -6JS + \frac{12JS + K}{2}\left[1 - \frac{(g\beta H/2)}{[K(12JS + K)]^{1/2}}\right]^2 . \tag{B.5c}$$

Equation (B.5c) clearly represents a maximum energy (which, in view of (B.4c), can occur only within a restricted range of H). Hence, to obtain the absolute minimum energy, we must compare (B.5a) and (B.5b). It follows immediately that

$$g\beta H = 2[K(12JS - K)]^{1/2} \tag{B.6}$$

defines a critical value of H, below which State I (defined by (B.4a) and (B.5a)) will be the lower energy state, and above which State II (defined by (B.4b) and (B.5b)) will have the lower energy.

In Figure 12, the energy (as expressed in (B.3)) has been plotted as a function of χ for different values of H; the unrealistically high value of 0.25 was chosen for K/12JS in order that the characteristics of equation (B.3) that are dependent on K, be brought out more distinctly. It is clear from this figure that for values of applied field other than those close to the condition for spin state transition, both States I and II may be expected to be reasonably stable. However, when the field is very near the critical value defined by (B.6), States I and II are favored about equally and are separated by a low energy barrier (see Figure 12). An expression for the height of this barrier is easily determined by the substitution of (B.6) into (B.5c); it is thus found that

$$\frac{(\Delta E)}{NS}_{\text{barrier}} = 12JS - [(12JS)^2 - K^2]^{1/2}$$
$$\simeq K^2/24JS \quad \text{for } K \ll 12JS. \tag{B.7}$$

In most physical cases of antiferromagnetic crystals, this energy barrier is so low that a small thermal energy is sufficient to overcome it. Consequently, transition between States I and II should take place very readily when the applied field is equal to the critical value defined by (B.6).

Let us now find the static equillibrium positions of the spin vectors when the field is applied perpendicular to the anisotropy axis. In this case, although the spin vectors must again lie in parallel planes due to the exchange forces between them, it is not immediately obvious that these planes must be parallel to both the anisotropy axis and the axis of the applied field. Hence, in a plane perpendicular to H, let us turn the K-axis through an arbitrary angle, ϕ, from its position shown in the spin vector diagram of Figure 13. With reference to this schematic diagram, the positions of the spin vectors in the plane of the applied field, are defined by the angles, χ and θ. The energy of this system may then be written as

$$E = -6NJS^2\cos 2\theta - \tfrac{1}{2}Ng\beta HS[\cos(\chi - \theta) + \cos(\pi - \chi - \theta)$$
$$+ \tfrac{1}{2}NKS(\sin^2\psi_1 + \sin^2\psi_2)$$

where $\cos\psi_1 = \cos\phi\cos(\frac{\pi}{2} - \chi + \theta)$, and $\cos\psi_2 = \cos\phi\cos(\frac{\pi}{2} - \chi - \theta)$.

or $$E/NS = 6JS(2\sin^2\theta - 1) - g\beta H\sin\theta\sin\chi$$
$$+ K[1 - \cos^2\phi(\sin^2\theta + \sin^2\chi - 2\sin^2\theta\sin^2\chi). \tag{B.8}$$

It follows from this last expression, that the energy is minimized with respect to ϕ when ϕ is set to zero. Hence, the two-dimensional schematic diagram of Figure 13 describes the system adequately for the remaining discussion. We proceed to find that (B.8) is minimized with respect to θ when

$$\sin\theta = \frac{(g\beta H/2)\sin\chi}{12JS - K(1 - 2\sin^2\chi)}, \tag{B.9}$$

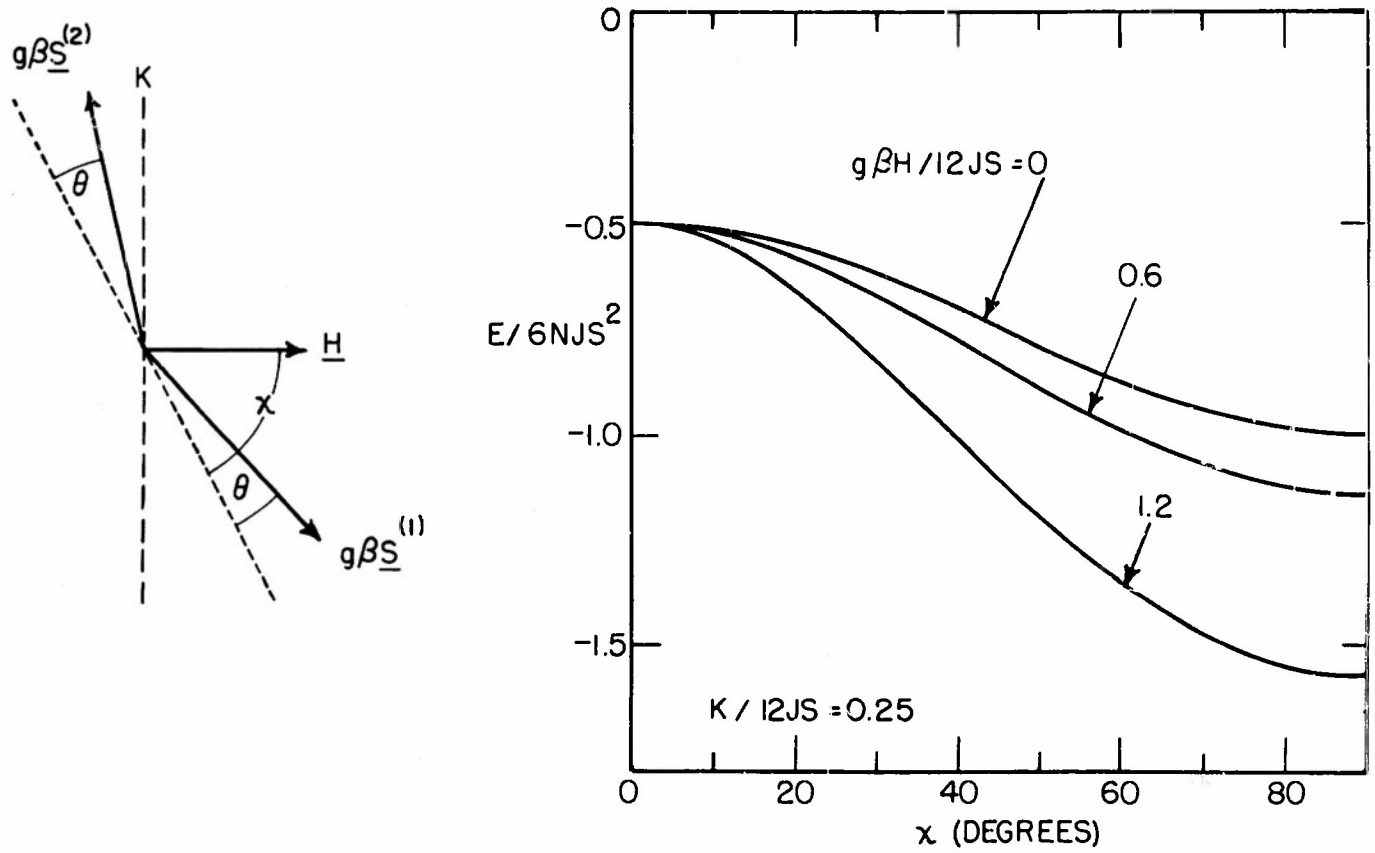
gβS(2)
K
θ
H
χ
θ
gβS(1)
0
gβH/12JS=0
-0.5
0.6
E/6NJS2
-1.0
1.2
-1.5
K/12JS=0.25
0
20
40
60
80
χ (DEGREES)

FIGURE 13

in which case, (B.8) becomes

$$E/NS = -6JS + K\cos^2\chi - \frac{(g\beta H/2)^2 \sin^2\chi}{12JS - K(1 - 2\sin^2\chi)} \qquad (B.10)$$

Finally, by differentiating (B.10) with respect to χ, we find that as long as $K < 12JS$, the energy is minimized by $\chi = \pi/2$, for any value of applied field. Thus, (B.9) and (B.10) are reduced, respectively, to

$$\sin\theta = g\beta H/2(12JS + K) \qquad (B.11)$$

and $$E/NS = -6JS - (g\beta H/2)^2/(12JS + K). \qquad (B.12)$$

For comparison with Figure 12, the energy (as expressed in (B.10)) has been plotted in Figure 13 as a function of χ for $K/12JS = 0.25$ and various values of H. Clearly, when the applied field is perpendicular to the anisotropy axis, only one spin state of the system is possible, and it is a stable static equilibrium state for any value of the applied magnetic field.

Our determination of the spin equilibrium states for the two directions of the applied field relative to the anisotropy axis, is similar but more exact than Néel's original analysis.[16] Recently, Gorter and Haantjes[26] in their study of this problem, postulated an anisotropic exchange interaction between adjacent spins and thus included the magnetic anisotropy energy implicitly in their expression for the exchange energy. Their results, nevertheless, are qualitatively similar to ours.

References

1. F. Keffer and C. Kittel, Phys. Rev. 85, 329 (1952); J. Ubbink, Physica 19, 9 (1953); R. K. Wangsness, Phys. Rev. 93, 68(1954); and references therein.

2. P. W. Anderson, Phys. Rev. 86, 694(1952); R. Kubo, Phys. Rev. 87, 568(1952); J. M. Ziman, Proc. Phys. Soc. A 65, 540 and 548 (1952); and references therein.

3. L. Néel, Ann. Physique 3, 137 (1948).

4. J. H. Van Vleck, Phys. Rev 52, 1178(1937).

References

5. C. Herring and C. Kittel, Phys. Rev. 81, 869(1951).

6. R. K. Wangsness, Phys. Rev. 91, 1085(1953).

7. F. Seitz, Modern Theory of Solids (McGraw Hill, New York, 1940), chap. 3, sec. 18.

8. H. B. Dwight, Tables of Integrals and Other Mathematical Data (Macmillan, New York, 1947), p. 201.

9. C. Møller, Z. Physik 82, 559(1933).

10. F. Bloch, Z. Physik 61, 206 (1930).

11. N. F. Mott and H. Jones, Theory of the Properties of Metals and Alloys (Oxford University Press, 1936), pp. 236-239.

12. T. Holstein and H. Primakoff, Phys. Rev. 58, 1098 (1940).

13. C. Kittel, Phys. Rev. 82, 565(1951).

14. Keffer, Kaplan, and Yafet, Am. J. Phys. 21, 250(1953).

15. H. B. Dwight, op. cit., p. 200.

16. L. Néel, Ann. Physique 5, 232(1936).

17. M. Fallot, Ann. Physique 6, 305(1936); Elliott, Legvold, and Spedding, Phys. Rev. 91, 28(1953).

18. E. C. Stoner, Proc. Roy. Soc. A 165, 372 (1938).

19. C. Guillaud and M. Roux, C. R. Acad. Sci. 229, 1133 (1949); C. Guillaud and H. Creveaux, C. R. Acad. Sci. 230, 1256 and 1458 (1950); R. Pauthenet, Ann. Physique 7, 710 (1952).

20. E. J. W. Verwey and E. L. Heilmann, J. Chem. Phys. 15, 174(1947); Verwey, Haayman, and Romeijn, J. Chem. Phys. 15, 181(1947); Shull, Wollan, and Koehler, Phys. Rev. 84, 912(1951).

21. C. Kittel, Introduction to Solid State Physics (Wiley, New York, 1953), chaps. 9 and 10.

22. R. Millar, J. Am. Chem. Soc. 50, 1875 (1928) and 51, 215(1929).

23. S. A. Friedberg, Physica 18, 714(1952).

24. J. W. Stout and M. Griffel, J. Chem. Phys. 18, 1455(1950).

25. van den Handel, Gijsman, and Poulis, Physica 18, 862(1952).

26. C. J. Gorter and J. Haantjes, Physica 18, 285(1952).

DISTRIBUTION LIST

Technical Reports

2	Chief of Naval Research (427) Department of the Navy Washington 25, D. C.
1	Chief of Naval Research(460) Department of the Navy Washington 25, D. C.
1	Chief of Naval Research (421) Department of the Navy Washington 25, D. C.
6	Director (Code 2000) Naval Research Laboratory Washington 25, D. C.
2	Commanding Officer Office of Naval Research Branch Office 150 Causeway Street Boston, Massachusetts
1	Commanding Officer Office of Naval Research Branch Office 1000 Geary Street San Francisco 9, California
1	Commanding Officer Office of Naval Research Branch Office 1030 E. Green Street Pasadena, California
1	Commanding Officer Office of Naval Research Branch Office The John Crerar Library Building 86 East Randolph Street Chicago 1, Illinois
1	Commanding Officer Office of Naval Research Branch Office 346 Broadway New York 13, New York
3	Officer-in-Charge Office of Naval Research Navy No. 100 Fleet Post Office New York, N. Y.

1	Chief, Bureau of Ordnance (Re4) Navy Department Washington 25, D. C.
1	Chief, Bureau of Ordnance (AD-3) Navy Department Washington 25, D. C.
1	Chief, Bureau of Aeronautics (EL-1) Navy Department Washington 25, D. C.
2	Chief, Bureau of Ships (810) Navy Department Washington 25, D. C.
1	Chief of Naval Operations (Op-413) Navy Department Washington 25, D. C.
1	Chief of Naval Operations (Op-20) Navy Department Washington 25, D. C.
1	Chief of Naval Operations (Op-32) Navy Department Washington 25, D. C.
1	Director Naval Ordnance Laboratory White Oak, Maryland
2	Commander U. S. Naval Electronics Laboratory San Diego, California
1	Commander (AAEL) Naval Air Development Center Johnsville, Pennsylvania
1	Librarian U. S. Naval Post Graduate School Monterey, California
50	Director Signal Corps Engineering Laboratories Evans Signal Laboratory Supply Receiving Section Building No. 42 Belmar, New Jersey

3	Commanding General (RDRRP) Air Research and Development Command Post Office Box 1395 Baltimore 3, Maryland
2	Commanding General (RDDDE) Air Research and Development Command Post Office Box 1395 Baltimore 3, Maryland
1	Commanding General (WCRR) Wright Air Development Center Wright-Patterson Air Force Base, Ohio
1	Commanding General (WCRRH) Wright Air Development Center Wright-Patterson Air Force Base, Ohio
1	Commanding General (WCRE) Wright Air Development Center Wright-Patterson Air Force Base, Ohio
2	Commanding General (WCRET) Wright Air Development Center Wright-Patterson Air Force Base, Ohio
1	Commanding General (WCREO) Wright Air Development Center Wright-Patterson Air Force Base, Ohio
2	Commanding General (WCLR) Wright Air Development Center Wright-Patterson Air Force Base, Ohio
1	Commanding General (WCLRR) Wright Air Development Center Wright-Patterson Air Force Base, Ohio
2	Technical Library Commanding General Wright Air Development Center Wright-Patterson Air Force Base, Ohio
1	Commanding General (RCREC-4C) Rome Air Development Center Griffiss Air Force Base Rome, New York
1	Commanding General (RCR) Rome Air Development Center Griffiss Air Force Base Rome, New York

2	Commanding General (RCRW) Rome Air Development Center Griffiss Air Force Base Rome, New York
6	Commanding General (CRR) Air Force Cambridge Research Center 230 Albany Street Cambridge 39, Massachusetts
1	Commanding General Technical Library Air Force Cambridge Research Center 230 Albany Street Cambridge 39, Massachusetts
2	Director Air University Library Maxwell Air Force Base, Alabama
1	Commander Patrick Air Force Base Cocoa, Florida
2	Chief, Western Division Air Research and Development Command P. O. Box 2035 Pasadena, California
1	Chief, European Office Air Research and Development Command Shell Building 60 Rue Ravenstein Brussels, Belgium
1	U. S. Coast Guard (EEE) 1300 E Street, N. W. Washington, D. C.
1	Assistant Secretary of Defe se (Research and Development) Research and Development Board Department of Defense Washington 25, D. C.
5	Armed Services Technical Information Agency Document Service Center Knott Building Dayton 2, Ohio

1	Director Division 14, Librarian National Bureau of Standards Connecticut Avenue and Van Ness St., N. W.
1	Director Division 14, Librarian National Bureau of Standards Connecticut Avenue and Van Ness St., N. W.
1	Office of Technical Services Department of Commerce Washington 25, D. C.
1	Commanding Officer and Director U. S. Underwater Sound Laboratory New London, Connecticut
1	Federal Telecommunications Laboratories, Inc. Technical Library 500 Washington Avenue Nutley, New Jersey
1	Librarian Radio Corporation of America RCA Laboratories Princeton, New Jersey
1	Sperry Gyroscope Company Engineering Librarian Great Neck, L. I., New York
1	Watson Laboratories Library Red Bank, New Jersey
1	Professor E. Weber Polytechnic Institute of Brooklyn 99 Livingston Street Brooklyn 2, New York
1	University of California Department of Electrical Engineering Berkeley, California
1	Dr. E. T. Booth Hudson Laboratories 145 Palisade Street Dobbs Ferry, New York
1	Cornell University Department of Electrical Engineering Ithaca, New York

1	University of Illinois Department of Electrical Engineering Urbana, Illinois
1	Johns Hopkins University Applied Physics Laboratory Silver Spring, Maryland
1	Professor A. von Hippel Massachusetts Institute of Technology Research Laboratory for Insulation Research Cambridge, Massachusetts
1	Director Lincoln Laboratory Massachusetts Institute of Technology Cambridge 39, Massachusetts
1	Signal Corps Liaison Office Massachusetts Institute of Technology Cambridge 39, Massachusetts
1	Mr. Hewitt Massachusetts Institute of Technology Document Room Research Laboratory of Electronics Cambridge, Massachusetts
1	Stanford University Electronics Research Laboratory Stanford, California
1	Professor A. W. Straiton University of Texas Department of Electrical Engineering Austin 12, Texas
1	Yale University Department of Electrical Engineering New Haven, Connecticut
1	Mr. James F. Trosch, Administrative Aide Columbia Radiation Laboratory Columbia University 538 West 120th Street New York 27, N. Y.
1	Dr. J.V.N. Granger Stanford Research Institute Stanford, California